COMPARISON OF STRUCTURE, PROPERTIES AND WEAR PERFORMANCE OF COATINGS APPLIED BY HIPIMS AND CAE PVD DEPOSITION METHODS DURING THE MACHINING OF DIFFICULT-TO-MACHINE ALLOYS

COMPARISON OF STRUCTURE, PROPERTIES AND WEAR PERFORMANCE OF COATINGS APPLIED BY HIPIMS AND CAE PVD DEPOSITION METHODS DURING THE MACHINING OF DIFFICULT-TO-MACHINE ALLOYS

BY

LUCA WATANABE REOLON, B.ENG.

A Thesis Submitted to the School of Graduate Studies in Partial Fulfilment of the Requirements for the Degree Master of Applied Sciences

McMaster University, Hamilton, Ontario, Canada

MASTER OF APPLIED SCIENCE (2020) McMaster University

(MECHANICAL ENGINEERING) Hamilton, Ontario, Canada

TITLE: COMPARISON OF STRUCTURE, PROPERTIES AND WEAR PERFORMANCE OF COATINGS APPLIED BY HIPIMS AND CAE PVD DEPOSITION METHODS DURING THE MACHINING OF DIFFICULT-TO-MACHINE ALLOYS

AUTHOR: Luca Watanabe Reolon, B. Eng., Mechanical Engineering

SUPERVISOR: Dr. Stephen C. Veldhuis

Department of Mechanical Engineering

McMaster University

NUMBER OF PAGES: xiii, 82

ABSTRACT

High Power Impulse Magnetron Sputtering (HiPIMS) comes as a new and promising PVD method for the development of high-performance coatings for cutting applications. This technique utilizes high energy and ionization which can produce a denser and stronger ceramic in comparison to traditional deposition techniques. Important coating characteristics that arise from this method such as enhanced hardness, adhesion, and less defects, can be applied when machining hard-to-cut materials. In this study, investigation of tool life and wear mechanisms, mechanical and physical properties of AlTiN coatings deposited on carbide tools by HiPIMS and Cathodic Arc Evaporation (CAE) were analyzed when machining Inconel 718 and Stainless Steel 304. Experimental turning tests were performed to evaluate tool life, and the wear mechanisms were analyzed by optical and scanning electron microscopy. Nanohardness, scratch test, fracture toughness and other methods were carried out to evaluate the coating properties. Impedance experiments were performed to determine the coating porosity and resistance to corrosion.

The results showed that HiPIMS coating presented higher hardness, toughness to fracture and adhesion to the substrate in comparison to CAE coatings. The HiPIMS coated tool substantially improved tool life when machining Inconel. The dominant wear mechanism found was abrasion, which is induced by the presence of hard carbides. The main wear patterns observed were flank, notch, and crater wear. The tool performance of HiPIMS was found to have enhanced mechanical properties, lower porosity, and form a larger amount of tribo-oxides when machining, in comparison to CAE.

ACKNOWLEDGEMENT

First and foremost, I would like to express my sincere thanks to my supervisor Dr. Stephen Veldhuis who`s expertise and guidance have made this thesis possible, and for the precious learning opportunity through the last two years.

In addition, I would like to thank Dr. Fox-Rabinovich for his invaluable role in the direction of this project through his vast knowledge of the subject area. I also wish to thank: Dr. Abul Arif for guiding and giving valuable inputs throughout the research; Dr. Jose Paiva for his guidance on conducting the experiments; Dr. Julia Dosbaeva for assisting in the coating characterization microscopy, and Dr. Igor Zhitomirsky for distinguished guidance with porosity experiments. I gratefully acknowledge the Canadian Network for Research and Innovation in Machining Technology (CANRIMT) for their support.

I would like to express a special thanks to all staff and colleagues at McMaster for continuous support, learning and friendship. My thanks are also extended to my colleagues Lucas, Max, Edinei and Pietro who have been by my side during this period.

To Dr. Fred Amorim and Dr. Michelle Meruvia for guiding and instructing me with valuable scientific research experience since during my undergrad.

To Dr. Giselle Munhoz, Dr. Adriano Moraes, and Dr. Marion Foerster for inspiring me to do science and enjoy the learning of physics since high school.

Finally, nothing would have been possible without the unconditional support of my family, in special my beloved mother Harumi, who always encourage me throughout all my years of study.

CONTENTS

LIST OF FIGURES

LIST OF TABLES

THESIS OUTLINE

This thesis is separated into 6 chapters which are briefly described as follows:

CHAPTER 1 – INTRODUCTION: In this chapter the motivation of this research is presented as well as the main research objectives.

CHAPTER 2 – LITERATURE REVIEW: In this chapter all the main concepts, theoretical references and other relevant research are presented with the objective of provide enough background for this study. This chapter can be separated into 4 main points: the process, the material, the tooling, and surface integrity of coatings.

CHAPTER 3 – EXPERIMENTAL PROCEDURE: The description of the methodology, experimental setups, test parameters and sampling are described in this chapter. The experimental procedure can be separated into four parts, workpiece characterization, cutting tests, surface integrity and corrosion tests.

CHAPTER 4 – RESULTS AND DISCUSSION: The results obtained by the experiments performed are presented followed by a detailed discussion.

CHAPTER 5 – CONCLUSIONS: In this chapter the main conclusions of the research will be stated and supported by the results achieved during the experiments.

CHAPTER 6 – SUGGESTIONS FOR FUTURE WORK: Based on the results achieved in this study other related aspects that can be investigated in future works will be identified and discussed in this chapter.

CHAPTER 1 – INTRODUCTION

1.1 BACKGROUND

Advances in manufacturing technology are mainly directed towards increasing the overall productivity of industrial processes. The chief demands come from manufacturers of light-weight parts, e.g., the automotive or aerospace industry. One way to reduce the weight without compromising the performance capacity, is to enhance the structural strength of material components. Materials such as stainless steel and nickel-based Inconel meet the demanding requirements associated with many applications but are difficult to machine and thus require advanced cutting tools.

The deposition of hard thin films of several micron thickness is a common means of improving the performance of tools, dies and molds for many different applications. Beginning with thermally activated chemical vapor deposition (CVD), different methods of coating application have been developed, including plasma-assisted physical vapor deposition (PVD). As such, coated tools offer better protection against mechanical and thermal loads, diminish frictional interactions between the tool and chip and improve wear resistance in a wide cutting temperature range compared to uncoated ones. The importance of wear-resistant hard coatings is highlighted by the following facts. Around 90% of all indexable inserts for metal cutting are based on cemented carbide substrates and are coated for wear protection by CVD or PVD techniques, with PVD being used in about 25% of the cases. What matters in the future is not which deposition technology is being used, but rather which properties can be achieved at what production cost. This is where the need for microstructural design enters the picture [2].

A relatively recent advance in PVD sputtering technology is High Power Impulse Magnetron Sputtering (HiPIMS) used for the physical vapor deposition of thin-film coatings based upon Magnetron Sputtering with a high voltage pulsed power source. HiPIMS utilizes a very high voltage, short duration burst of energy focused on the target coating material to generate a high-density plasma that results in a high degree of ionization of the coating material in the plasma. In HiPIMS, power densities are very high, producing energetic ions that compact the coating as it grows, creating very dense coatings. Coatings deposited by HiPIMS do not have the porosity found in conventional techniques and deliver a better surface finish and corrosion resistance [3].

In terms of coating chemical composition, the most extensively investigated coating system involves (Ti, Al)N, due to its well-established deposition parameters and ease of compositional adjustment, as well as its potential to enhance the tools' cutting performance. Although enhancing the aluminum content would improve the coatings' oxidation resistance, the PVD process is restricted by the deposition of insulating films composed of approximately 65– 67 mol.% AlN.

1.2 MOTIVATION

To enhance machining productivity and increase cutting tool life, a thin film hard coating can be applied by a physical vapor deposition (PVD) technique [2]. In industry, such coatings are typically deposited by cathodic arc evaporation (CAE), due to its high deposition rate, high current density, and the enhancement of the coating layer's mechanical properties. However, one of the disadvantages of this method is the production of liquid metal droplets with sizes of 100–1000 nm on the coated surface [3]. These types

of defects can reduce the tool's life. HiPIMS is a relatively new PVD method with a high energy and plasma ionization rate that can produce denser and stronger ceramic coatings for cutting tool applications compared to traditional techniques [2]. It is capable of producing an extremely dense plasma with a high ionization rate and high pulsed peak ion current density, to deposit a dense coating layer with a columnar structure and very low void concentration. The HiPIMS method can generate a high proportion of metal ions (a metal/ion ratio of up to 1:1) without creating droplets because it is essentially a sputtering method [3]. All of these indications support the idea that HiPIMS coatings can improve the life and quality of cutting tools during machining.

1.3 RESEARCH OBJECTIVES

The aim of this work is to investigate the differences between HiPIMS and CAE coatings and compare their performance during machining. Specifically, the research objectives of this work are described as follows:

1. Comprehensive characterization of the coatings.
2. Comparative tool wear studies of CAE deposited AlTiN coatings vs. HiPIMS during the turning of Inconel 718.
3. Comparative tool wear studies during the turning of Stainless Steel 304.

CHAPTER 2 - LITERATURE REVIEW

2.1 PHYSICAL VAPOUR DEPOSITION (PVD)

The application of coatings on a cutting tool is an effective way of improving machining process productivity through the enhancement of tool performance. This technique enhances wear resistance and facilitates the friction and sliding between the tool and the chip.

The choice of the deposition method depends on process requirements, such as coating/workpiece material, type of machining operation, etc. Examples of such principal methods are: electroplating, spray coating, CVD and PVD [1]. In general, the term "coating" refers to layers of a microscopic (10^{-6} meters) thickness or more, whereas "thin film" is applied to a layer whose width can range between several microns down to a few atomic thicknesses [2].

The PVD deposition process is composed of the vaporization of a source in the form of atoms or molecules which are carried through a vacuum chamber, where they condense on a target surface. The mechanisms of source material evaporation are either thermal activation or collisional bombardment. Thermal evaporation and vacuum evaporation heat the source material until its atoms/particles are expelled from the target surface, and thus become available for deposition. Collisional bombardment involves gas ions (inert gases such as He, Ar, reactive gases such as N, O or simple hydrocarbons) accelerated by plasma that transfer momentum and eject particles from the target surface [3]. Chemical compounds such as TiN, AlO can be generated whenever reactive gases are employed.

Both CAE and HiPIMS studied in this research involve collisional bombardment with the employment of plasma.

The mechanism of plasma ionization, also known as electron impact ionization (Fig. 1), is characterized by the collision of a primary accelerated electron and atom, which overcomes the ionization potential to produce a positive ion and two secondary electrons:

$$Atom + \ e^{-} \rightarrow Ion + 2e^{-}$$

This state is maintained until the two electrons produced by ionization are accelerated by an electric field and collide with subsequent atoms, creating a chain reaction [2], [4].

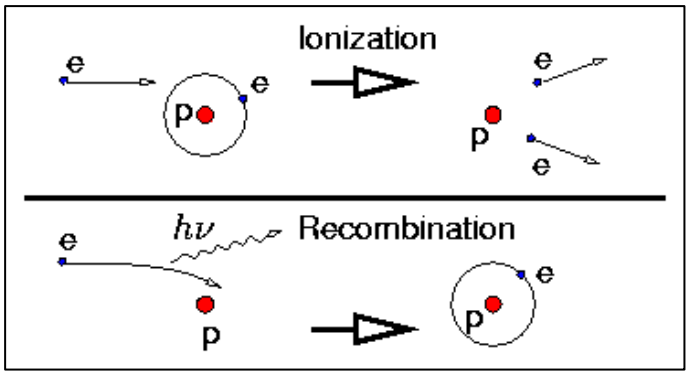

Figure 1 - Ionization and recombination scheme [5]

Recombination occurs between an electron and an ion which combine to form a neutral atom, satisfying the laws of conservation of energy and momentum. Other types of collisions (interactions) that occur in plasma are elastic, excitation, attachment, and dissociation. An electric field is induced into the process to maintain the production of ions and electrons, due to the process of recombination which creates neutral particles not useful for deposition purposes.

The working temperatures of the PVD process are at the lower range required for deposition, around 450-550°C [5]. The degree of plasma ionization for coating applications is typically only 10^{-4} [4] with the gas mostly consisting of neutral particles. Since collisions between ions and electrons are ineffectual, the ions can only receive some of the energy from the external electric field. The low temperature condition creates gradients or inhomogeneities throughout the thickness of the film. This in turn, enables control of features such as the managed synthesis of phases and structures in the form of nanolaminate, nanocolumnar materials [5].

Recent advances in PVD techniques are mainly focused on increasing the energy densities in order to produce denser and thinner coatings with improved machining characteristics. Denser coatings have become possible through the application of pulsed plasma and an increase of the potential bias between the electrodes [3]. Deposition methods also can be studied in terms of their own parameters and substrate characteristics. For example, one of the most important coating properties is adhesion, which can be improved by altering substrate morphology features such as grain size and roughness (not only just the deposition parameters).

The PVD technique produces coatings that are on average, 5 μm thick, which is less than traditional CVD processes that deposit coatings in the thickness range of 20 μm. As such, CVD methods usually perform better in roughing operations subjected to abrasive wear whereas PVD is more appropriate for finishing operations where a sharp cutting edge is important. CVD has the disadvantage of subjecting the tool substrate to a higher processing temperature, normally between 800°C and 1200°C, which can promote an

annealing process in some materials, e.g., HSS substrates [7]. PVD can also produce sharper edges than CVD due to its ability to control the coating thickness on the cutting edges [3]. The importance of this properties was noted earlier.

2.2 CATHODIC ARC EVAPORATION

Cathodic arc evaporation (CAE) with a high ionization rate, is the most widespread technique used to fabricate hard nitride coatings that exhibit strong adhesion to various substrates and dense microstructures with stoichiometric composition [5], [11]. However, macro-particle growth defects that increase the surface roughness [13] and contribute to the fast-outward diffusion of substrate materials [12] are inevitable, which limits the high precision applications of arc-evaporated AlTiN coatings.

In CAE, the arc current varies from 300-400 A for titanium, causing arc erosion due to a combination of melting and evaporation of molten and solid particles.

The use of magnetically filtered cathodic arc evaporation can suppress the macro droplet defect to a certain extent, at the expense of the deposition rate [14]. Nevertheless, the relatively high residual stress generated during CAE, primarily as a consequence of energetic particle bombardment during deposition, limits the applications of thick AlTiN coatings.

2.3 HiPIMS

HiPIMS is a PVD-method capable of achieving extremely dense plasma with a high ionization ratio and high pulsed peak ion current densities [6]. This method provides

superior film properties such as dense and smoother films as well as enhancing film substrate adhesion [7].

There is a sharp voltage peak in HiPIMS (500 – 3000 volts) at a very high peak power (up to 3000 W/cm^2) and a low duty cycle (0.5 – 5%) that gives an average power similar to a continuous dc magnetron sputtering process (e.g., 3 Wcm^2). This provides the vaporized material with high ionization, but the sputtering rate is reduced when compared to a continuous dc magnetron sputtering process operating at the same power [8]. One of the main advantages of HiPIMS over CAE is the high amount of ions present in the plasma (up to 90% in the plasma [1], [9], [10]).

Kulkarni et al. [7] compared HiPIMS with a cathodic arc evaporation (CAE) technique for stainless steel 304 that had a 4 μm AlTiCrN coating. The tool life was reported to be 40% longer when deposited using HiPIMS as compared to a coating prepared by CAE. One of the chief reasons for this improved performance was attributes to the superior adhesion of the AlTiCrN (HiPIMS) coating on the substrate. In addition, the AlTiCrN HiPIMS coating generates a more stable and protective alpha phase film on the surface, which helps to enhance the performance of the cutting tool. Helmersson et al. [11], developed a nanoscale multilayer TiAlCN/VCN coating of about 2.2 nm, deposited by HiPIMS for machining applications. It was stated in their study that the coating had a clean and sharp coating/substrate interface of 5 nm thickness, which resulted in very high coating adhesion corresponding to Lc = 58 N. During the dry milling of an Al 7010-T 7651 alloy, the TiAlCN/VCN nanoscale multilayer PVD coating outperformed state of the art DLC, Cr/WC/α-CH coated and uncoated end mills by factors of 4 and 8, respectively.

Nanocrystalline HiPIMS coatings promote rapid diffusion of aluminum to the surface along the grain boundaries. This results in the fast formation of an alumina surface protective layer that significantly reduces the sticking of the stainless steel to the tool's surface due to the high chemical and thermal stability of the alumina layers. The thermal conductivity of the tool surface layers is reduced as well. Therefore, a greater amount of heat enters the chips and becomes dissipated via chip removal. It is also possible that a reduction of work-hardening occurs during stainless steel machining due to the formation of alumina tribo-films. This eventually reduces the intensity of attrition wear and significantly improves the tool life.

Major drawbacks of this technique are its high energy demand, which affects its cost, as well as its low rate of deposition. The impediment to machining productivity due to such limiting factors can be outweighed if an improvement in tool life can be achieved using this technique. This requires a more thorough study of its effect on the wear performance.

2.4 COATING ASPECTS

A widely used family of ceramic coatings for machining applications is $(Ti_{1-x}, Al_x)N$ due to its strong oxidation resistance and thermal stability [3]. Under elevated temperatures, oxide Al_2O_3 tribo-films are formed on the coating surface, acting as a diffusion barrier [5]. Recent research efforts seeking to increase x by a factor of greater than 0.5, resulted in improved hardness, oxidation resistance and tool life of the coated cutting tools, since substitution of Ti atoms with smaller Al atoms reduced the lattice

parameter of the deposited coating layer [14], [15]. HiPIMS enables the relatively easy deposition of an AlTiN coating with high Al content via the sputtering method. AlTiN coatings have excellent thermal stability, superior mechanical properties, and high oxidation resistance in comparison to traditional TiN coatings for cutting tools. The presence of aluminum diffused on the surface along the grain boundaries results in the rapid formation of an Al_2O_3 surface protective layer through interaction with the environment. The thermal conductivity of the tool surface was reduced by alumina as well, preventing the concentration of heat on the tool. Since HiPIMS coated tools are expected to have longer tool life during machining than traditional methods, one of the major goals of this study is to find a causal relationship between the material's structural characteristics and its cutting process performance.

2.4.1 X-Ray Diffraction

Ceramic coatings based on Ti-Al-N are one of the most widely used materials for tool life improvement, due to their high wear resistance and high adhesion to the substrate. Adhesion is crucial during machining since very high pressures and temperatures are present in the cutting zone which promote delamination of the coating. The resistance of the coating can be evaluated by different methods, as determined by its application. Hardness is the most important parameter in metal cutting due to the nature of the cutting process itself [12]. A harder material is needed to cut the workpiece, so elements such as Titanium and Tungsten are used, they are normally present in the oxide and carbide states. These states are significant in that they provide chemical stability during machining.

Diffusion is one of the most important wear mechanisms of machining, so improvements have been developed for oxide coatings that act as a barrier between the tool and the workpiece [13].

Baumvol et al. identified several phases in TiAlN films through XRD, including intermetallic phases (Ti_3Al, Ti_9Al_{23}) and ternary phases ($Ti_3Al_2N_2$, Ti_3AlN, Ti_2AlN) that were found in the TiAlN solid solution [16]. However, the majority of structures found on the coatings are solid solutions TiN, Ti_2N and AlN. TiN has a cubic atomic structure, Ti_2N is tetragonal and at a low hydrostatic pressure, AlN has a hexagonal structure. Schuler et al. reported that TiAlN films have three separate phases, which are: a NaCl-type solid solution for $0 < x \leq 0.58$, a wurtzite-type solid solution for $0.83 \leq x < 1$, and an intermediate phase belonging to the hexagonal system in the vicinity of $x = 0.7$. [17]. Therefore, coatings with $x \cong 0.6$ are used in this study to ensure that the expected structure is of a cubic Na-Cl type.

Elmkhah et al. compared coatings deposited by HiPIMS with different bias voltages [18]. XRD 2-theta, lattice parameter, crystalline size, texture, and residual stresses were determined for 50, 100, 150 and 200 V bias voltages. A stress tester machine (J&L Advanced Plasma Technology™) works by applying a laser to the surface to estimate residual stress. JADE6.5 software was used to assess the lattice strain values.

The chemical composition of the deposited coatings was modified by increasing the bias voltage as shown on Fig. 2. This phenomenon can be attributed to the “re-sputtering” effect caused by the difference between the atomic mass of Ti and that of Al, which is lighter.

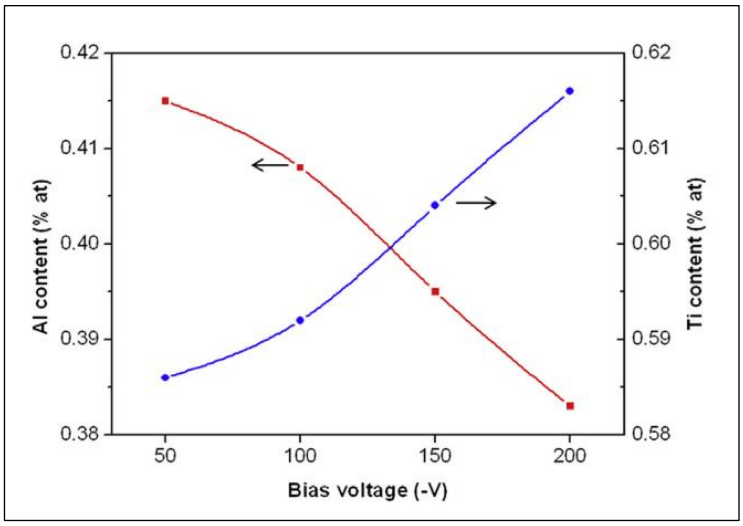

Figure 2 - Chemical composition of the -50 V to -200 V coatings for different voltages [18].

X-ray diffraction patterns revealed that the preferred orientation of crystalline planes were of (111), (200), (220) and (222) with respective diffraction angles of: 37.2°, 43.3°, 63.0° and 80.0°, as shown in Fig. 3. The coating's main orientation of (111) of 50 V had changed to (200) as the bias voltage grew to 200 V. This can be explained by the fact that the atomic radius of Al is smaller than the atomic radius of Ti, so the interplanar distance (d) decreased once the Al atoms were incorporated within the TiN lattice in the form of a solid solution.

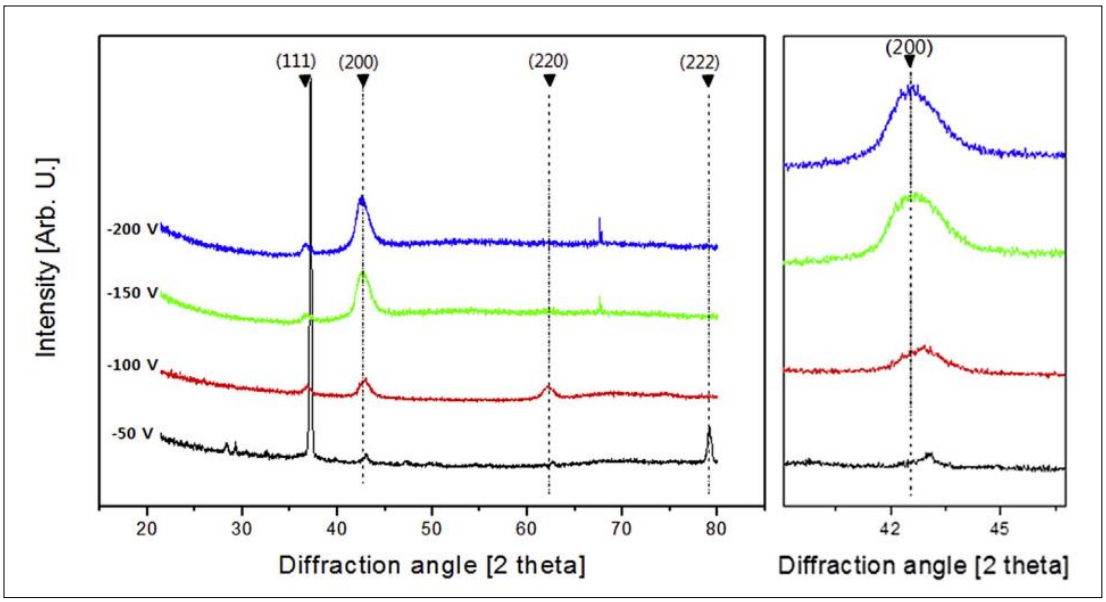

Figure 3 - XRD diffraction of samples with different voltages [18].

The calculated diffraction patterns can be obtained from the CIF database for the different phases of this material. In this application, it was found that according to Fig. 4, the cubic pattern of TiN was very similar to that measured in Fig. 3, indicating the presence of a solid solution containing Al atoms in its structure. Other structures such as Ti_2N and AlN were compared but did not exhibit similar peaks.

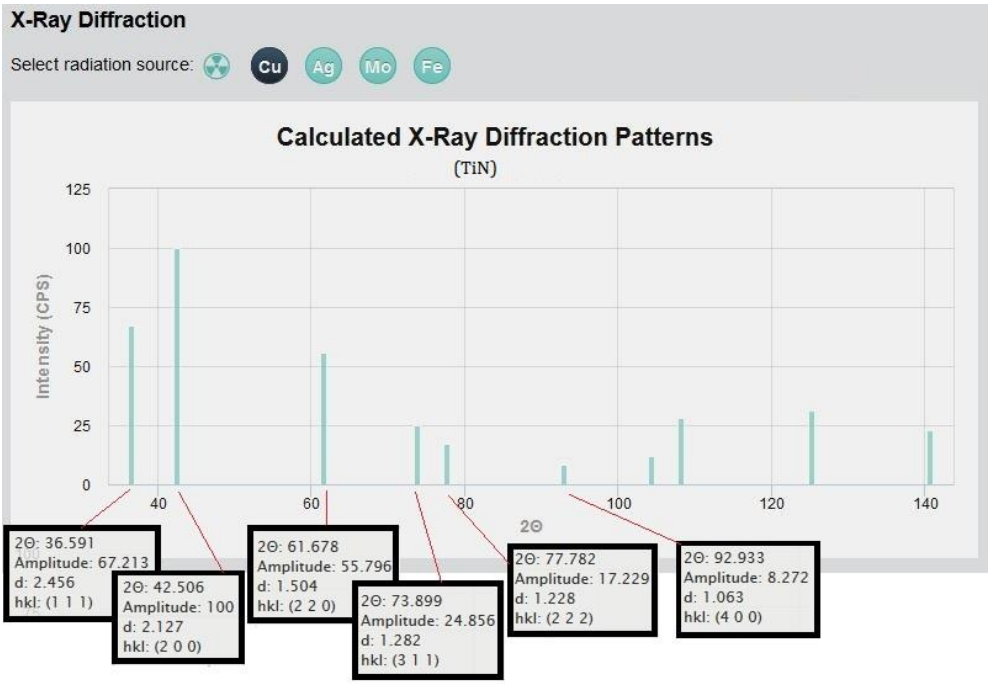

Figure 4 - The calculated diffraction pattern of TiN from the CIF database. [19]

It was also found that a greater number of defects could result from enhanced ion bombardment and the re-sputtering effect at a high bias voltage. The defects in the sputtered film inhibit the migration of grain boundaries and cause the formation of smaller grains. In addition, more surface defects increase the number of preferential nucleation sites, which may also lead to a decrease in the crystallite sizes. The average crystallite size of TiAlN coatings was calculated from the Williamson-Hall relation [20]. Surface defects can appear if the process parameters are not optimized, resulting in an increase of the number of preferential nucleation sites, which can also reduce the crystallite size.

2.4.2 Porosity

To develop optimized coating systems, fast and reliable methods of porosity characterization are important in evaluating the efficacy of the deposition process.

Electrochemical impedance spectroscopy (EIS) has been proven useful for studying the localised corrosion of coating/steel systems and offers many advantages over conventional electrochemical polarisation techniques.

Electrochemical techniques have been used to characterize the corrosion behavior and porosity of PVD coatings by several authors [1-5]. Ahn et al. [1], studied Cr/CrN and CrAlN multilayer coatings applied to WC. The trends of porosity as a function of immersion time were evaluated by electrochemical impedance spectroscopy (EIS). It was found that an accurate porosity measurement depended strongly on the correlation between the porosity enlarged ratio and the charge transfer resistance, which determined the critical time. Tato (1998) et al. [2] evaluated Ti and duplex TiN coatings on brass using three different methods. The first method of assessing porosity consists of a comparison between the DC polarization resistances of a coated and an uncoated substrate at a constant potential. Alternatively, the degree of porosity could also be represented by the ratio of current maxima observed during dissolution of the brass substrate with or without a coating. Fan (2016) et al. [3] analyzed TiN and CrN PVD coatings on mild steel and AISI 316L stainless steel after the coated systems were immersed in a 0.5% NaCl solution. Constant phase elements that represented the non-ideal characteristics of the electrochemical interface were designated as Q. They were introduced to improve the accuracy of the simulation and to account for the mass transport behaviour through the introduction of diffusion related elements such as Warburg and cotangent hyperbolic impedance. The inclusion of these parameters significantly improves the extent to which the simulation fits EIS data. Ananthakumar et al. [4] studied TiN, TiAlN and TiN/TiAlN multilayers deposited by DC

magnetron sputtering with a focus on the corrosion resistance of coatings and the relationship between physical and mechanical properties such as roughness, friction coefficient. The multilayer coatings were found to have superior corrosion resistance and improved mechanical properties. Zhang et al. [5] studied the corrosion resistance of three coatings and the substrate immersed in a 3.5% NaCl solution at 25°C. Based on the electrochemical data, AlCrSiWN featured a higher corrosion resistance than AlCrN and AlTiN.

Table 1 - Literature Review on EIS of coatings

Researcher	Method	Composition	Thick [um]	Porosity [%]	Solution
Fan, 2016	Arc ion plating	AlTiN (40/60)	3	12.27	3 % NaCl
Liu, 2002	Arc ion plating	TiN & CrN	2.5	0.14	0.5% NaCl
Ananthakumar, 2011	DC magnetron sputtering	TiN/TiAlN multilayer	2	0.12	3.5% NaCl
Zhang, 2015	Cathodic arc evaporation	AlTiN	3	4.63	3.5% NaCl
Tato, 1998	DC magnetron sputtering	Ti and TiN	2	0.5	0.67 M NaCl

Electrochemical impedance theory describes the response of a circuit to voltage or an alternating current as a function of frequency [6]. The total impedance in a circuit is the combined opposition of all its resistors, capacitors, and inductors to the flow of electrons. The chief theoretical advantage of this method is that it can use a purely electronic model to represent an electrochemical cell, the interface of which is analogous to an electronic circuit consisting of a specific combination of resistors and capacitors that can be correlated

to an impedance plot obtained with its equivalent theoretical circuit. Impedance is a measure of resistance to electric current without the limitations given by Ohm's law:

$$E = R * I \qquad \text{(Eq. 1)}$$

Using Ohm's law, a DC potential (E) can be easily applied to a circuit, for measuring the resulting current (I), computing the resistance (R), or determining any term of the equation if the other two are known. Potential values are recorded in volts (V), where the EIS measurement consists of applying an AC potential to an electrochemical cell and then analyzing the resultant current flowing through it via Fourier series.

The film porosity (F) was analyzed by a method described in the literature using the following equation:

$$F = \frac{R_{pm}}{R_p} \times 10^{-\,|\,\Delta E/\beta\,|} \qquad \text{(Eq. 2)}$$

where ΔE is the corrosion potential difference of the uncoated and coated substrates, β and R_{pm} are the respective anodic Tafel slope and the polarization AC resistance of the uncoated substrate, and R_p is the polarization AC resistance of the coated substrate. Fig. 5 shows the electrical model used in this study.

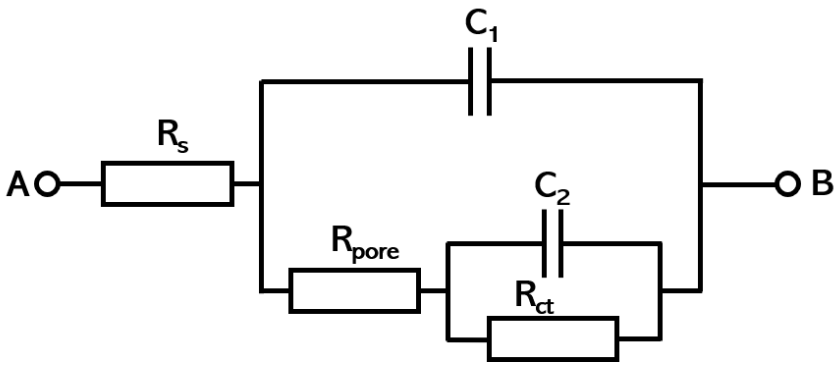

Figure 5 - Equivalent electrical circuit for EIS data of the substrate and AlTiN coating that was corroded in a 3.5 wt.% NaCl solution

The total polarization resistance (Rp) is composed of the resistance of the coating (including the pores) and the resistance of the interface between the defective site and the substrate.

$$R_p = R_{pore} + R_{ct} \qquad \text{(Eq. 3)}$$

In the equivalent circuit, the electrolyte resistance characteristics are presented as follows [3]:

- R_s is the resistance of an electrolyte solution between the working electrode and the reference electrode.
- C_2 is the double-layer capacitance related to the electrochemical process occurring between the alloy and the solution.
- R_{ct} represents the charge transfer process that occurs between the alloy and the electrolyte. In the AlTiN coating, the equivalent circuit contains two additional elements, the capacitance C_1 and the charge transfer resistance R_{pore} caused by the formation of an ionic conduction path through the coating.

- The corrosion interface is characterized by a parallel capacitor with a double-layer constant phase element C_2 and charge transfer resistance R_{ct}.

Note that C represents the constant phase element, which is responsible for the deviation from the ideal dielectric behavior of a non-ideal capacitor. The goal of this study is to investigate the relation of the coating's mechanical properties with its performance through the EIS experiment described in Fig. 6.

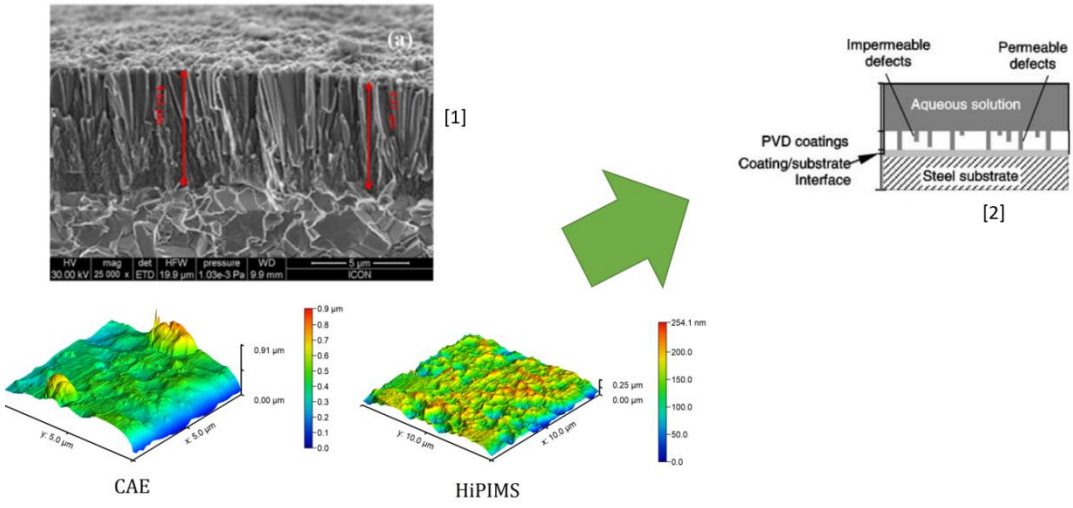

Figure 6 - The proposed relationship between a coating's mechanical properties and its performance in the EIS experiment [1-2].

AlTiN coatings applied on a WC substrate through PVD, have columnar structures, within which columnar and point defects can be produced. In PVD coatings, porosity and growth defects may result from unfavorable growth conditions, substrate imperfections or the presence of dust particles. The presence of pores and pinholes in the coatings is indirectly indicated by the measurement of the EIS properties of the coatings. These electrochemical measurements vary due to the presence of pores in the coatings as they provide a passage for the exposed substrate to react chemically or electrochemically with a

corrosive environment [1]. Whenever a coating has pores, the polarization result is a combined output of the coating and the substrate, therefore this technique overestimates the porosity of the coatings. An electrical equivalent circuit with double layer capacitance is thus used to account for this discrepancy. If the pores are either closed or only wide enough to allow for some specific ions or molecules in the electrolyte to gradually migrate to the substrate surface, these are termed as closed pores. Zheng (2002) et al. [7] applied this concept on DLC thin films to analyze each different case.

Diffusional impedance is primarily related to the microstructure of coatings. A columnar structure (e.g., for TiN) contains more open (through coating) porosity and straight grain boundaries [25]. These defects can provide efficient diffusion channels for reactive species. Thus, for TiN coated steel (MS or SS) systems, Warburg impedance is employed to represent semi-infinite length diffusion. However, a non-columnar (e.g., equiaxed) crystallite structure (e.g., CrN) has less open porosity [25]. Diffusion of reactants in the CrN coating must take a zigzag route, such that the diffusion process becomes slow and difficult. Therefore, a cotangent–hyperbolic diffusion impedance (O) is used to represent finite length diffusion. The related details regarding the use of diffusional elements are discussed in a paper by Diniz et al. [28].

The presence of a pore and pinhole in the coatings is indirectly indicated by the measurement of the through pores in the coatings under study. Initially, the coating's porosity remains relatively constant (Step I). This region observed just before Step II indicates the actual porosity. There is a drastic increase of porosity after the first step. The

difference of chemical composition tends to preferentially perpetrate through coating defects.

The oxidation tends to propagate through coating defects. Therefore, the galvanic corrosion cell was then established as localized corrosion began to dominate. In conclusion, factors that affects impedance are presented:

- The rough surface is not only a result of insufficient polishing and corrosion, but also of dislocations, grain boundaries, and impurities.
- A columnar structure (e.g., for TiN) contains more open (through coating) porosity and straight grain boundaries.
- Internal closed pores.
- Materials chemical behaviour (e.g., Chemical passivation).

2.5 DIFFICULT-TO-MACHINE ALLOYS

2.5.1 Inconel

Summary of issues associated with the machining of Inconel 718:

1. High strength at high temperatures, poor thermal conductivity, work hardening [5-7].
2. Presence of (hard) carbide phases (TiC, NbC, MoC, CrC, etc.) at grain boundaries [8,12,13].
3. Presence of high mechanical and thermal stresses during machining, along with oxidation [5-8].

4. Dominant failure modes (wear patterns) are severe flank, notch, and crater wear [9,10].
5. PVD coatings are normally used to improve productivity to enable machining speeds of over 50 m/min (cutting speeds below 30 m/min are employed for uncoated tools) [5,6,7].
6. Coatings are susceptible to chipping, fracture on edges, or removal due to poor adhesion [2-5].

Nickel-based superalloys such as Inconel 718 (IN 718) have been widely used in aircraft engines, nuclear reactors, and land-based gas turbines mostly due to their capacity to maintain thermal stability and high strength at high temperatures [5], [6]. IN 718 is considered a difficult to machine material due to its strength hardening at elevated temperatures. Its hardness increases along with a rise in temperature up to 650°C [7]. The presence of a quantity of super hard carbide phases (TiC, NbC, MoC, CrC, etc.) at the grain boundaries can produce a continuous and intensive shock load, resulting in abrasive wear on the cutting tools [8]. A highly durable (tough) tool coating will be more likely to resist the intermittent shocks during the cutting process [9]. The poor thermal conductivity of Inconel can generate very high temperatures (up to 1000°C) on the rake face of the cutting tool. Therefore, machining of this material is associated with low cutting speeds, short tool life and consequently high production costs. The primary tool wear mechanism during the machining of this material is adhesion with built up edge (BUE) formation.

2.5.2 Stainless Steel

Workpiece materials with elevated strength and stiffness contribute to a high tool wear rate, considering their intense operating conditions in the machining industry. Therefore, the development of tools with enhanced tool life is essential for ensuring greater machining productivity. One of the most commonly used techniques for tool improvement is the application of hard coatings. Coated tools combine the strength properties of the bulk material and the surface characteristics possible when using a deposited coating. This combination enables the production of complex machined parts made from IN 718 and other difficult to cut materials.

2.6 MACHINING SOLUTIONS

Techniques such as near-dry machining, also known as minimum quantity lubrication (MQL) and cryogenic machining have been shown to offer promising improvements to tool life and machined surface integrity. Marques et al. investigated the addition of graphite and MoS2 solid lubricants to vegetable oil based commercial cutting fluid during the turning of Inconel 718 under a MQL method [5]. A tool life improvement of 46% was observed resulting from the addition of MoS2 to the coolant as compared to the use of pure commercial oil Musfirah et al. [10] when milling IN 718 [7]. In the same study dry and cryogenic conditions were also studied with surface roughness, cutting forces and microstructural alterations (including undesirable carbide inclusions on the workpiece) ended up being lower during cryogenic machining than dry machining. However, tool life in the cryogenic environment was shorter than that in dry cutting. The extremely low

temperatures associated with using liquid nitrogen as a coolant can change the properties of the cutting tool materials, which leads brittleness and more cracks forming on the tool edge due to the shock load generated during milling [7]. Other methods of tool life improvement to consider are coatings applied onto cutting tools, high pressure coolant and cryogenic cutting laser assisted machining.

2.7 RESEARCH GAPS

The main scientific contributions that this work seeks to achieve are:

- To find evidence for a causative relation between the mechanical and physical properties with the machining performance of HiPIMS.
- To perform detailed studies using XRD diffraction to study coating deposition parameters and conduct an impedance test to evaluate the coating porosity.

CHAPTER 3 - METHODOLOGY

A schematic diagram is presented in Fig. 7 showing all experiments in this study.

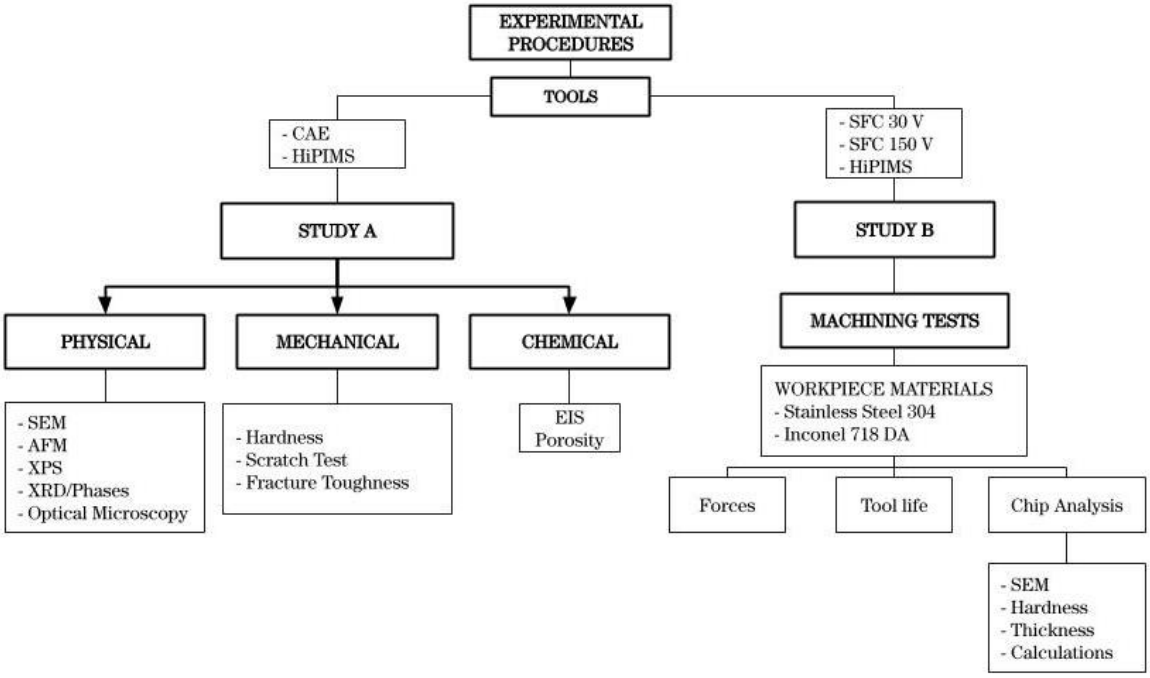

Figure 7 - General overview of experiments for this research.

The experimental procedures used include the following:

- Physical Characterization: SEM and EDS analysis were done on a Vega Tescan 3 microscopy. An optical microscope Keyence VHX-6000 was used to collect 3D images of wear on cutting tools. The XRD diffraction patterns were analyzed on an AXRD Benchtop Powder X-ray Diffractometer by Proto Manufacturing. A copper beam (1.5444 A) with a target power of 30kV (20 mA) was employed. For AFM measurements, an Anton Paar Tosca 400 was used, and allowed the determination of roughness and surface morphology.

- Mechanical Characterization: The nanohardness experiment was performed on an Anton Paar NHT3 Nano-Indentation Platform. Progressive loads from 0 to 40 mN were applied at 40 different spots. A Berkovich Diamond indenter was used in this study. The adhesion and fracture toughness were determined by an Anton Paar scratch tester, which has the capability to determine critical loads and length of fractures.
- Chemical Characterization: Electrochemical characterization was performed using a potentiostat-impedance analyzer PARSTAT 2273 (Ametek) in 3% NaCl aqueous solution with 3-electrode corrosion cells containing a working electrode (uncoated or coated substrate), counter-electrode (Pt mesh) and a reference saturated calomel electrode (SCE). The results of potentiodynamic studies (1 mV s^{-1} rate) were presented using Tafel plots. EIS data was obtained using alternating current (AC) in the frequency range of 0.01Hz-10 kHz and voltage amplitude of 5 mV. The EIS data was presented in Bode plots.

The cutting performance tests were represented by:

- Tool life: this step consists of cutting tests experiments to determine the performance of each coating in terms of tool life, wear mechanisms and wear patterns. Tool life experiments determine which tool last longer during intermittent machining, the wear mechanisms analysis show what types of wear occurred by the machining process and the wear behaviour analysis indicated how the tool wears during cutting. This step was done to evaluate the wear resistance of the coatings,

using the failure criteria of 300 μm on flank wear (ISO 3685) in terms of cutting length as measured using optical microscopy analysis. A finish turning operation was performed under a wet condition with Speed = 350 m/min, Feed rate = 0.1225 mm/rev, Depth cut = 0.5 mm for SS 304 and Speed = 60 m/min, Feed rate = 0.1225 mm/rev, Depth cut = 0.25 mm for IN 718.

- Chip analysis: analysis of morphology and surface by SEM, hardness, and chip ratio determination with calculation of other cutting variables. Shear bands were also observed by SEM.

3.1 WORKPIECE PROPERTIES

The chemical composition and mechanical properties of both Austenitic Stainless steel 304 and Inconel 718 used are presented in Table 2.

Table 2 - Chemical composition of workpieces used in this study.

Chemical composition of SS 304							
Element	Cr	Ni	Mn	Si	C	P	Fe
wt. %	18.7	8.05	1.8	<0.75	<0.08	0.02	Bal.

Mechanical properties

Hardness (MPa)	Yield strength (MPa)	Tensile strength (MPa)	Elongation (%)
660	205	515	40

Chemical composition of IN 718							
Element	Ni	Cr	Fe	Nb	Ti	Al	Fe
wt. %	51.7	19.5	18.9	4.9	1.4	1.1	Bal.

Mechanical properties

Hardness (MPa)	Yield strength (MPa)	Tensile strength (MPa)	Elongation (%)
1138	1034	1275	12

For study B, IN 718 direct aged (DA) was used instead of regular IN 718 which was used in Study A. The chemical composition is the same but mechanical properties are different. The properties of IN DA 718 are presented in Table 3.

Table 3 - Mechanical properties of IN DA718

Inconel DA718	Hardness (HRC)	Yield strength (MPa)	Tensile strength (MPa)	Elongation (%)
	45	1230	1490	21

3.2 MACHINING EXPERIMENTS

The tool life experiments were performed on an Okuma Crown-S (Study A) and Boehringer VDF 180CM Lathe (Study B). In the machinability tests, cemented carbide inserts (CNGG120402FS, Kennametal) with a rake angle of 12°, clearance angle of 0°, and nose radius of 0.2 mm, were used with different coatings applied as outlined in Table 4. NC stands for Normal Cathode while SFC stands for Super Fine Cathode, with both being CAE methods. The dimensions of the test specimen were Ø70×300mm. A semi synthetic oil fluid with 6% concentration was used as a coolant. Piezoelectric dynamometer (Kistler 9257A) was used to record forces. The experiments were performed with a maximum spindle speed of 3000 rpm.

Table 4 - Coatings used in this study.

Sample	Manufacturer	PVD method	Study
KC 5010	Kennametal, United States	NC (CAE)	A
HiPIMS	Balzers, Germany	HiPIMS	A and B
30V and 150V	MMRI McMaster, Canada	SFC (CAE)	B

The machining parameters chosen for this study are summarized in Table 5.

Table 5 - Cutting parameters for machining tests

Method	***Inconel 718***	***Stainless Steel 304***
Speed [m/min]	60	350
Feed rate [mm/rev]	0.1225	0.1225
Depth of cut [mm]	0.25	0.5
Condition	Finishing	Finishing
Coolant	Wet	Wet

3.2.1 Performance and selection of cutting parameters

A matter of even greater significance than commercial application, is to gain an in-depth understanding of the physics of HiPIMS in relation to the coating properties generated which resist wear mechanisms of machining. In this study, the experiments were conducted under standard ISO 3685, which considers tool failure at reaching 300 µm of wear at the flank face of the cutting tool. The amount of wear present on the other faces are not considered on the cutting failure for this standard. The machining process and the wear mechanisms involved are a very complex set of phenomena during which a great amount of pressure and very high temperatures are generated at the tip of the tool. It is vital to understand all the process variables, considering that slight changes in the variables can lead to big changes in tool life.

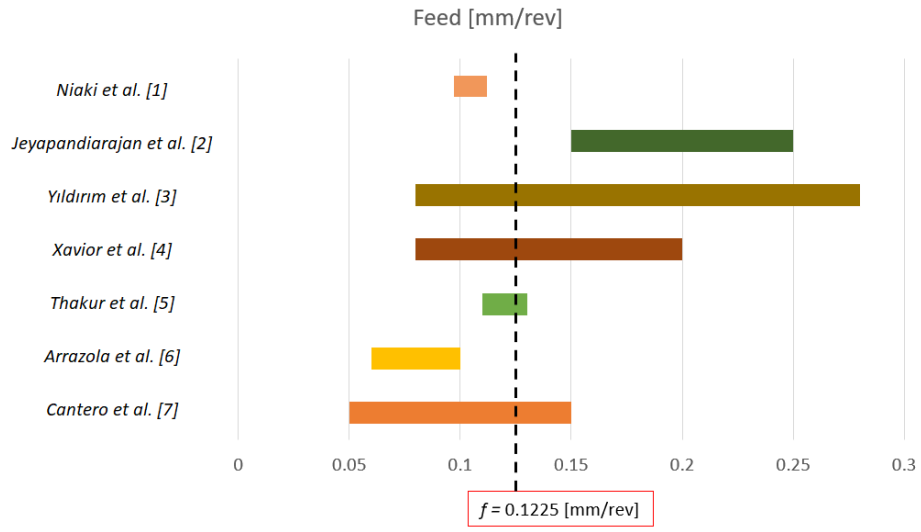

Figure 8 - Selection of feed based on literature.

The parameters used for this study are the average or most representative parameters used in scientific practice, which enables the cross-checking of results. AlTiN

coatings deposited on carbide substrates during the machining of In718 served as the experimental samples in this work. The finishing operation was conducted at a feed of 0.1225 mm/rev and cutting speed of 60 m/min.

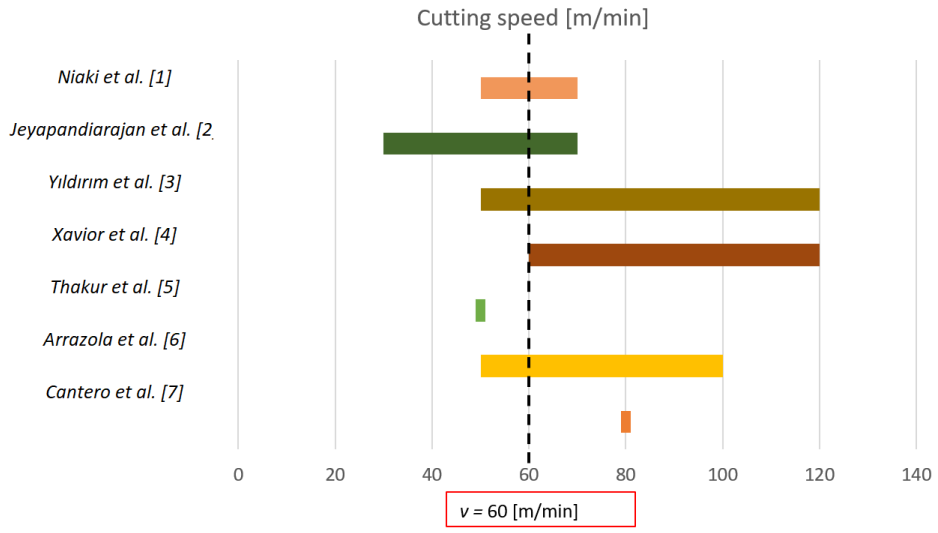

Figure 9 - Selection of cutting speed based on literature.

The coating thickness parameters were determined from the data made available by commercial AlTiN coating manufacturers. Whereas deposition by arc cathode is limited to a max coating thickness of ~6 μm, HiPIMS is capable of depositing a coating layer of up to 12 μm thick. A fixed thickness of 4 μm was chosen for this study.

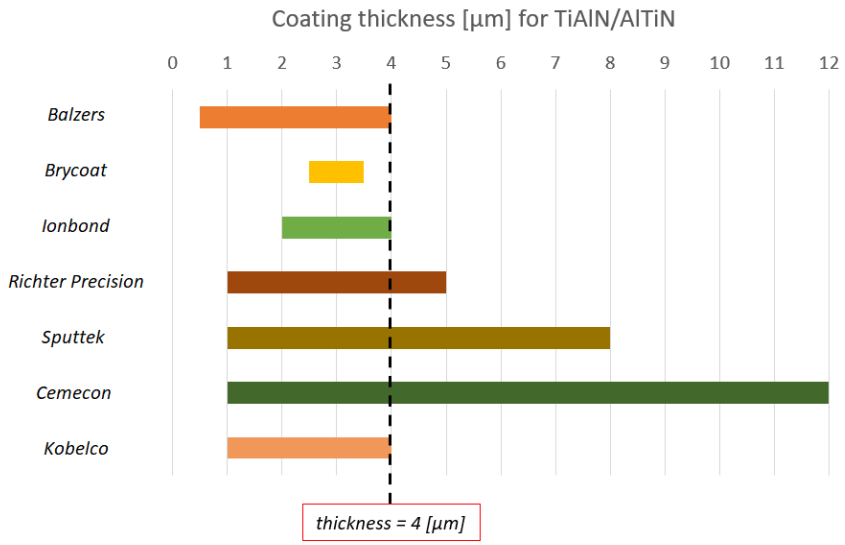

Figure 10 - Selection of thickness based on companies.

Liu et al. [12] have reported that forces could be reduced by increasing the cutting speeds to 90 or 120 m/min (heat softening) although at the cost of an increase in temperature. This may indicate the presence of high cutting forces at low cutting speeds. The poor thermal conductivity of Inconel can generate very high temperatures (up to 1200°C at high speeds) on the rake face of the cutting tool. Therefore, machining of this material is associated with low cutting speeds, short tool life and ensuing high process costs. The primary tool wear mechanism is then adhesion with BUE formation [4]. Continuous chips were produced at higher cutting speeds without traces of a BUE, which accounted for the lower surface roughness of the end product. The surface roughness increased alongside the feed rate. The depth of flank wear progression was found to have increased along with the cutting speed. Lower cutting forces were observed on the coated tool compared to an uncoated one, this was attributed to the low friction coefficient and superior adhesion properties of the coating. Fernández et al. [4] studied the machining behavior of AISI 303 austenitic SS at a very high speed. The study concluded that at a

higher cutting speed, the cutting force and surface roughness have increased as well. The machined surface produced at a high speed was found to be superior to the surface produced at a low speed, judging by the feed marks and presence of surface defects. Nayak et al. [5] reported a higher material removal rate with decreased cutting force and surface roughness at the lowest cutting velocity while investigating the influence of various cutting parameters on the machining of AISI 304 austenitic stainless steel with an uncoated carbide insert. Junaidh et al. [6] reported that flank and crater wear are the predominant tool wear mechanisms in this case. The increased ductility of the work material resulted in the production of continuous chips. Temperature variation throughout the thickness of the chips caused the formation of curly chips. It was concluded that the cutting forces diminished as the cutting speed was gradually raised.

3.3 PROPERTIES CHARACTERIZATION

The phase characterization chemical compound of the coatings was analyzed by an X-ray photoelectron spectroscopy (XPS) on a Physical Electronics (PHI) Quantera II spectrometer (Chanhassen, MN, USA).

The adhesion strength between the coating and the substrate was determined by an Anton Paar Revetest Scratch Tester. The critical lengths were defined as:

- Lc1 – position where the first crack appeared.
- Lc2 – position where it was possible to see the substrate for the first time.
- Lc3 – position where the coating was completely removed.

The XRD diffraction patterns were analyzed by an AXRD Benchtop Powder X-ray Diffractometer by Proto Manufacturing. A copper beam (1.5444 A) with a target power of 30kV (20 mA) was employed. For AFM, an Anton Paar Tosca 400 was used.

CHAPTER 4 - RESULTS AND DISCUSSION

4.1 STUDY A – STRUCTURE AND PROPERTIES

The chief aim of this study was to identify the main structural, physical-chemical, and mechanical differences between CAE and HiPIMS methods of AlTiN coating deposition. The influence of these properties on the wear performance observed during the machining of hard-to-cut materials. Inconel 718 and Stainless Steel 304 were used as typical hard-to-cut workpiece materials for the experiments performed under finish turning conditions.

Topics in this chapter:

- SEM/AFM coating surface characterization
- Mechanical properties of the coatings
- XPS data
- XRD studies
- EIS studies
- Flank wear measurement data during the machining of an IN 718 alloy and SS 304 stainless steel

4.1.1 SEM/AFM coating surface characterization

Fig. 11 shows SEM data for both the CAE and HiPIMS coating surface. Droplets and porous defects of a few micrometers are typical for a CAE coating, as indicated in the left image. The HiPIMS coating, on the right side, exhibits a smoother surface with no clearly visible defects.

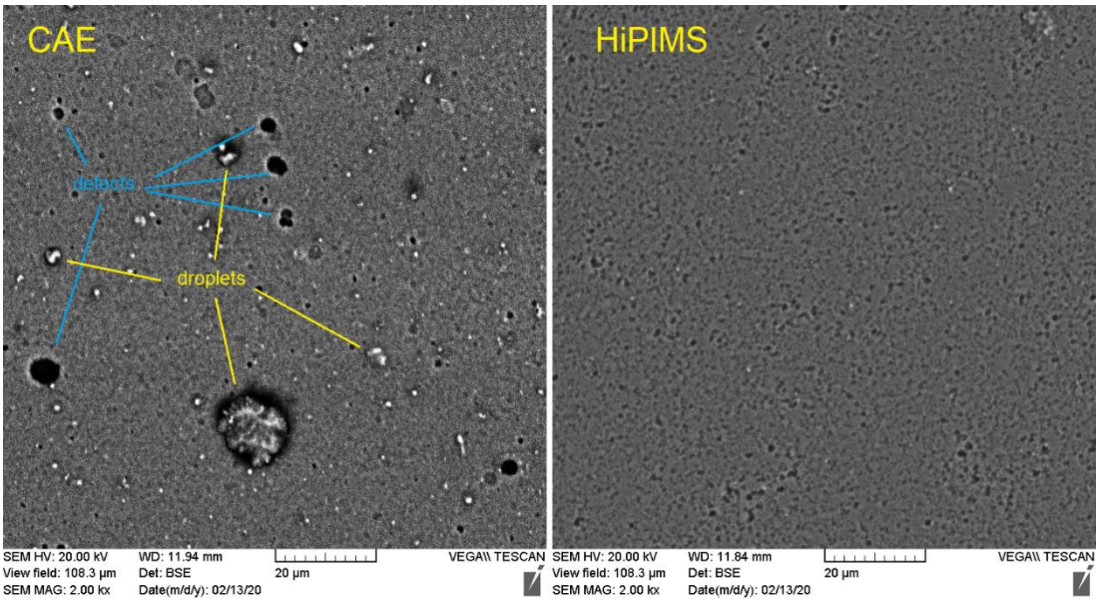

Figure 11 - SEM of coating surface morphology.

Fig. 12 presents the AFM images of both coatings. The presence of droplets was indicated in the CAE coating in the form of the higher peaks, whereas those of HiPIMS appear smoother which is consistent with the SEM images shown in Fig. 11.

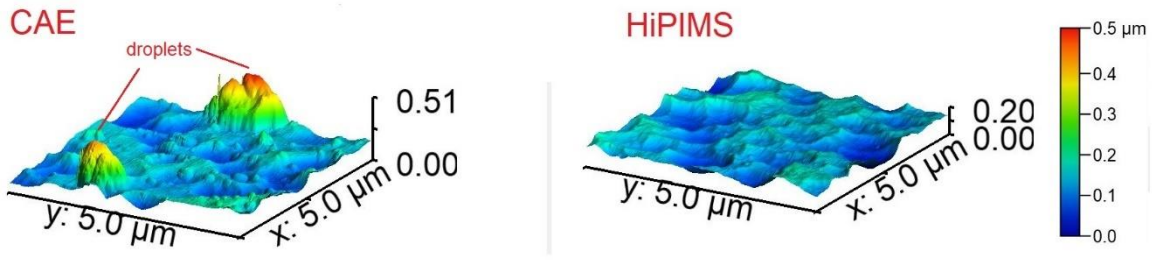

Figure 12 - AFM of coatings surface.

Table 6 shows the composition (atomic %) of Al and Ti, thickness, and roughness data for all coatings. The measured results show minor differences. The measured mean roughness of the CAE coating was 55 nm, whereas for HiPIMS it was 33 nm, confirming the SEM observations regarding the presence of droplets and defects on the surface.

Table 6 - Properties of the coating used in this experiment.

Coating	%Al atomic	%Ti atomic	Thickness (μm)	Roughness (nm)
CAE	56.7	43.3	4.7 ± 0.3	55 ± 1
HiPIMS	61.2	38.8	4.02 ± 0.3	33 ± 1

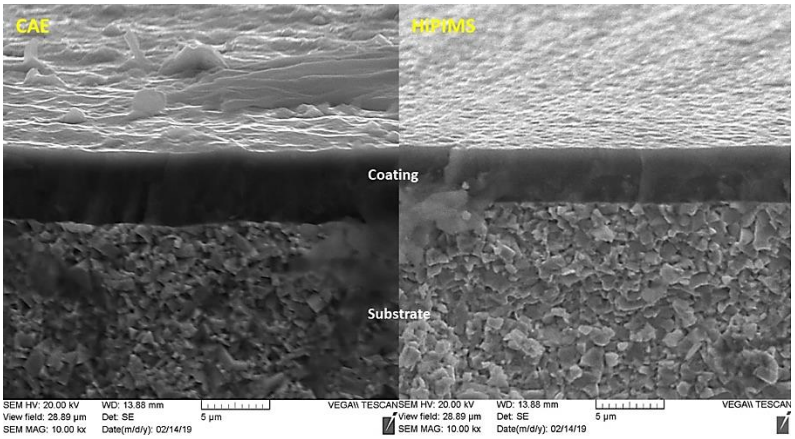

Figure 13 - SEM of cross section of coatings: CAD on the left, HiPIMS on the right.

4.1.2 Mechanical properties of coatings

Mechanical properties such as nanohardness, elastic modulus, fracture toughness, and critical loads of scratch test are plotted in Table 7.

Table 7 - Mechanical properties of the coatings.

Coating	Hardness (GPa)	Elastic modulus (GPa)	H/E	H^3/E^2	Lc1 (N)	Lc2 (N)	Lc3 (N)	Palmquist fracture toughness	Residual stresses (GPa)
CAE	37.4	610	0.061	0.368	40.4	50.6	53.9	0.213	1.88
HiPIMS	42.9	615	0.069	0.418	59.8	73.6	77.3	0.277	1.61

Both coatings have similar nano-hardness values. The HiPIMS coating had a roughly 20% higher fracture toughness than the CAE coating. Similarly, in table 8, the critical load Lc1 (appearance of the first crack) is around 30% higher in the HiPIMS coating. This indicates its higher adhesion to the substrate in comparison with that of the CAE coating. Lc2 and Lc3 values are also higher in the HiPIMS coatings.

SEM images from fracture toughness experiments are shown in Fig. 14. The crack propagation appears to be less intensive in HiPIMS than in CAE.

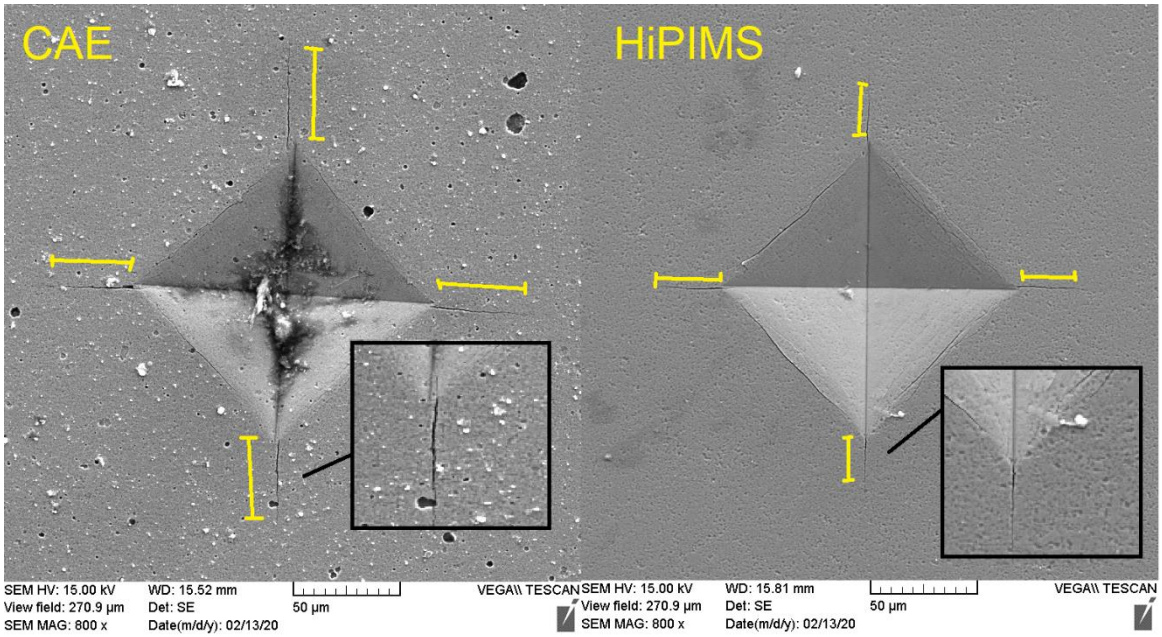

Figure 14 - SEM of fracture toughness experiment.

4.1.3 XPS

XPS data analyzing tribo-phases formed on the surfaces of both coatings during machining are presented in Fig. 15. HiPIMS features a higher amount of the sapphire tribo-phase, which may benefit machining performance as suggested in previous studies by Paiva et al. [21].

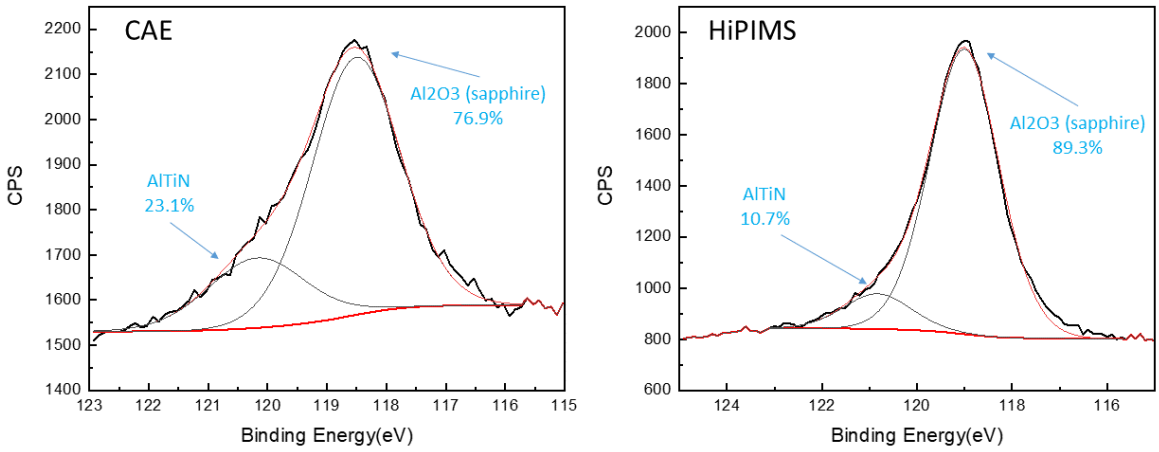

Figure 15 - XPS of AlTiN coating for two different coatings.

4.1.4 EIS

Fig. 16 shows Tafel plots for uncoated and coated substrates. Coated samples were shown to have a lower anodic current. Therefore, Tafel plots indicate that HiPIMS coatings feature strongly reduced levels of porosity, which was confirmed by SEM data. They also provided the substrates with better corrosion protection, as shown as follows:

- CAE, 0.58% porosity.
- HiPIMS, 0.12% porosity.

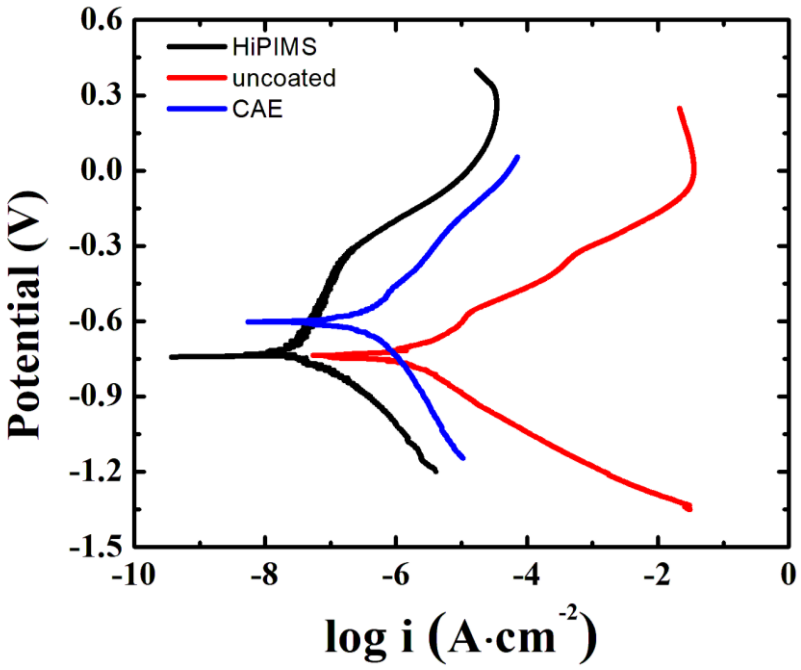

Figure 16 - Tafel plots for (a) uncoated and coated substrates: (b) third sample and (c) second sample

The protective properties of the coatings were also studied by the EIS method. Fig.17 depicts Bode plots for the uncoated and coated substrates. EIS studies showed increased impedance |Z| in the coated samples, which confirmed that the coatings acted as diffusion barriers for electrolyte ions.

- The corrosion current density of the AlTiN coating was lower than that of the substrate, which was taken to be an indication of its superior corrosion resistance.
- The nitride coatings were observed to form thin passive oxide layers on their surface when the coated samples were submerged in a NaCl solution [3].

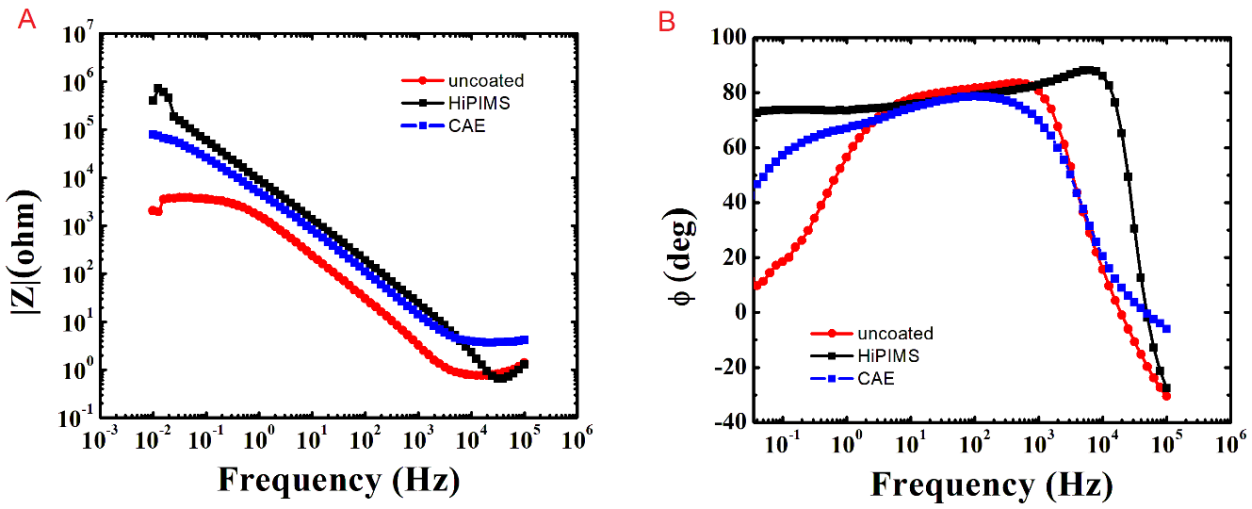

Figure 17 - EIS Bode plots of impedance Z versus frequency, (B) phase angle versus frequency for (a) uncoated and coated substrates (b) third sample and (c) second sample

As shown in Fig. 18, the absolute impedance of the HiPIMS coating is much larger than that of the CAE, which also implies that the HiPIMS coating possesses superior corrosion resistance than the substrate [3]. The abrupt drop by the end of experiment (at high frequencies) do not interfere in terms of the coating application since such stages of corrosion are not reached during the cutting process. EIS experiments last considerably longer than interaction between coated tool and chip. During cutting process, high rotation is employed, so the most representative part is at low frequencies.

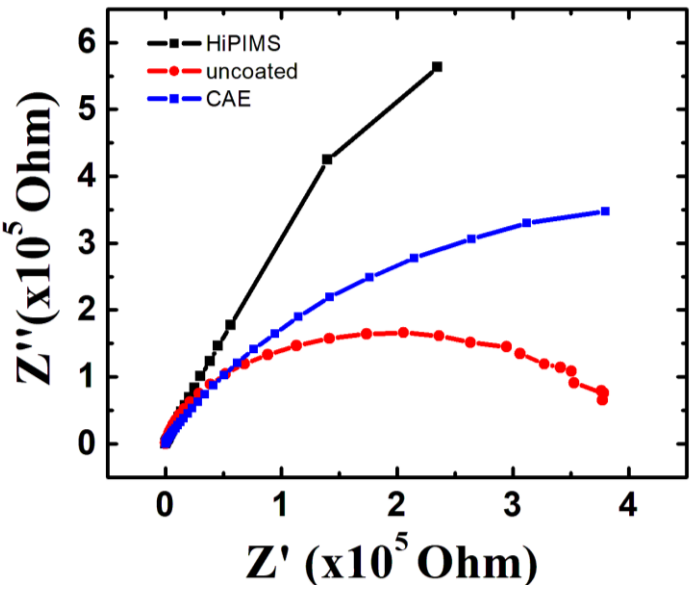

Figure 18 - Electrochemical impedance spectroscopy (EIS) of the substrate and an AlTiN coating in a 3 wt.% NaCl solution

In general, the larger the diameter of the capacitive loop, the better the corrosion resistance of the sample [3], in which the slope was higher. The results showed a high slope for HiPIMS, indicating better corrosion resistance than that observed for CAE.

4.1.5 XRD

Fig. 19 shows the XRD diffraction pattern of both coatings. The preferred orientation of both coatings was (200), with small differences in their intensity.

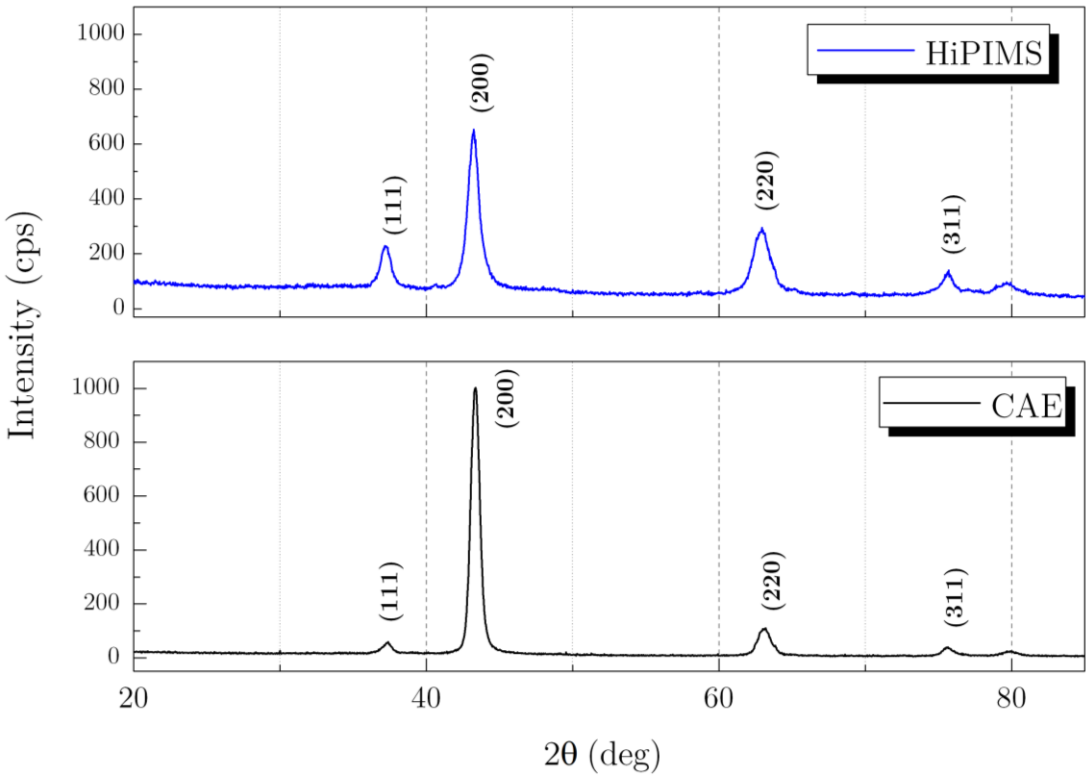

Figure 19 - Xray diffraction pattern for different coatings.

The crystalline size (c.z.) was predetermined for the main (200) orientation (Fig. 20). The standard reference value of the (200) peak in a TiN FCC B1 type structure was (42.633), as specified in the Joint Committee on Powder Diffraction (JCPDS, 87-0633). This value was an indication of a better organized structure with lower crystalline sizes in comparison to shifted values.

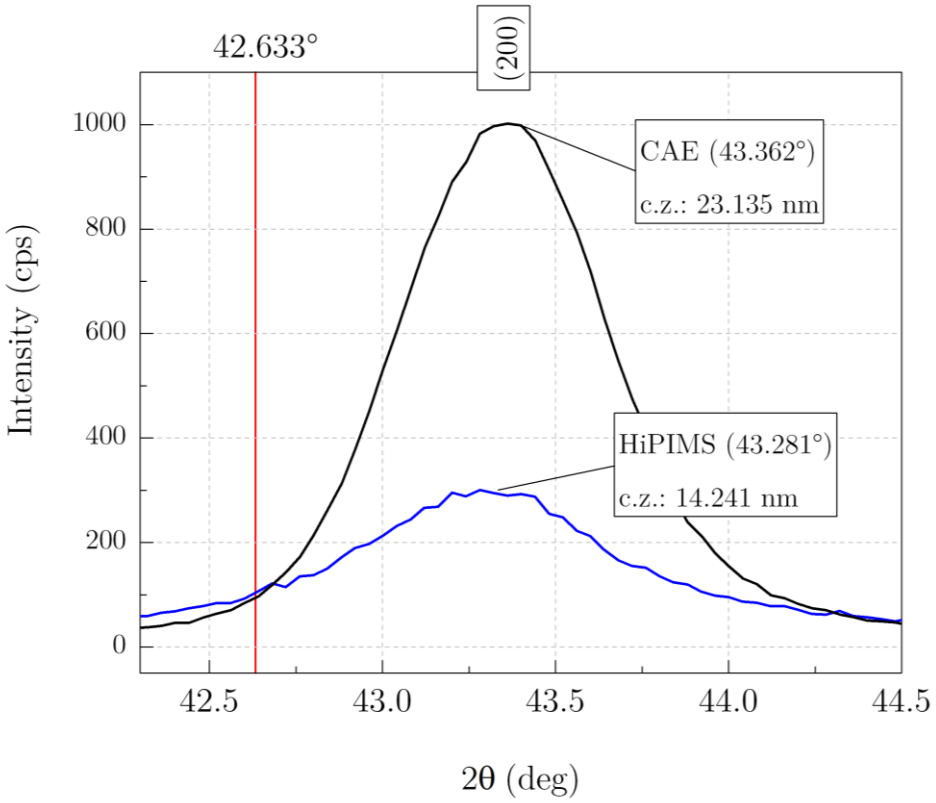

Figure 20 - Close look to Xray diffraction patterns.

The comparably high amount of Al, (which has a lower atomic radius than Ti), was observed to reduce the crystalline sizes as well.

4.1.6 Flank Wear vs. length of cut

Fig.21 shows the tool life result data collected during the machining of Inconel 718. The data presented show that the HiPIMS coating had a higher tool life. This can be a consequence of the higher strength, better adhesion, and presence of sapphire tribo-films on the friction surface. All these factors were observed to have an impact on the machining performance of the coating layer.

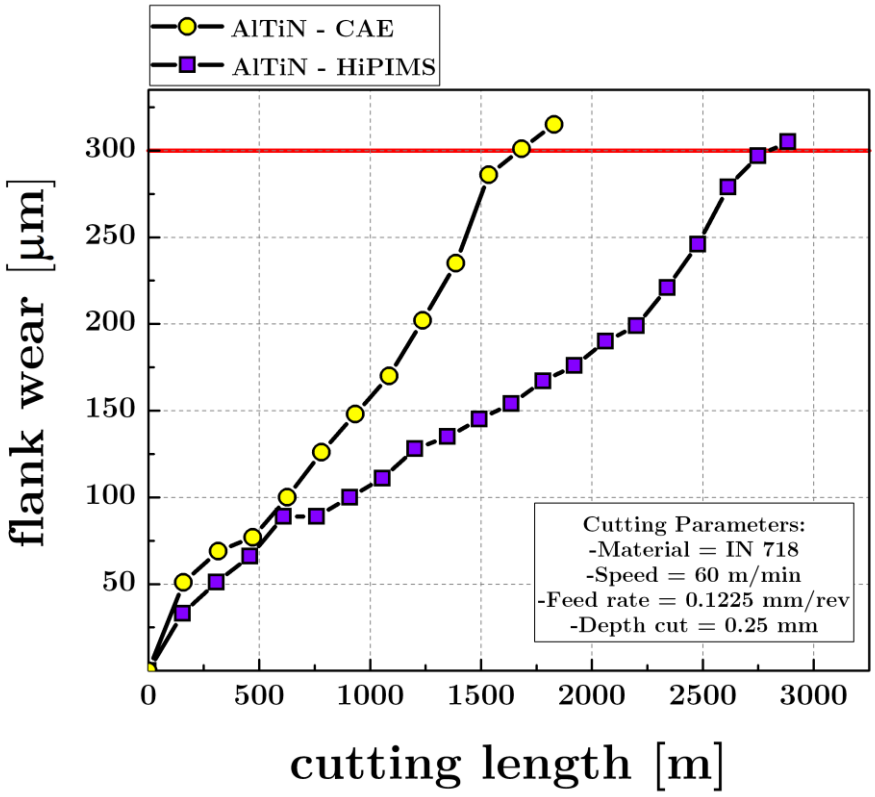

Figure 21 - Flank wear vs. length of cut during machining of Inconel 718 alloy.

Fig. 22 shows the results of a typical tool life experiment carried out during machining of Stainless Steel 304. These case studies exhibited an opposite trend to that of Inconel machining. The HiPIMS coating performed worse than CAE. The next chapter

follows up with a more detailed machining study to find the reasons for this unexpected behavior.

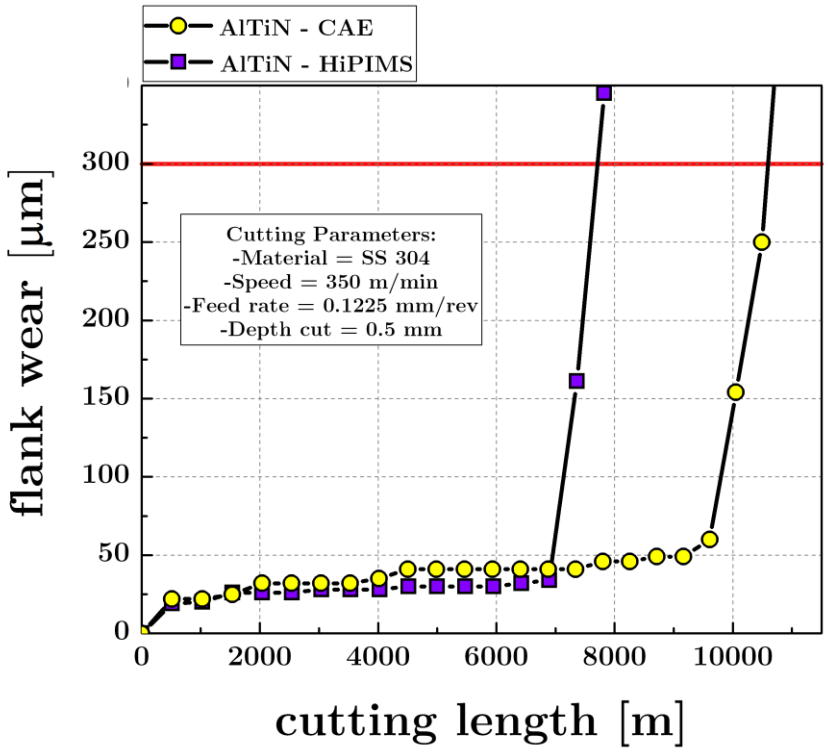

Figure 22 - Flank wear vs. length of cut during machining of SS 304.

4.1.7 Conclusions of Study A

The physical, mechanical, and chemical properties of the CAE and HiPIMS deposited coatings analyzed in the current study, can be summarized as follows:

- The coating deposited by the HiPIMS method had a smoother surface, lower number of defects and possessed superior mechanical properties ((higher adhesion, hardness) than those of the CAE deposited coating.

- Porosity studies revealed the presence of a higher percentage of pores in CAE coatings than in a HiPIMS deposited coatings, of which can be related to the presence of droplets forming on the tool surface during CAE deposition.
- The HiPIMS coating generated a higher amount of sapphire tribo-films, which facilitated chip flow and increased the tool life.

4.2 STUDY B - WEAR PERFORMANCE DURING THE MACHINING OF HARD-TO-CUT MATERIALS

This study was focused on the wear performance of coatings during the machining of hard-to-cut materials such as Inconel 718 DA and 304 Stainless Steel using cutting tools with AlTiN coatings deposited by CAE under varying deposition parameters (bias voltages of 30V and 150V) as well as the HiPIMS method. The CAE method used in study B is also called Super Fine Cathode (SFC) due to its more refine ionization than the traditional technique. These coatings were tested under finish turning conditions. Topics in this chapter include:

- Flank wear, Notch wear
- Volumetric wear/adhesion progression
- Forces
- Optical microscopy studies of the worn cutting tools
- SEM chips

4.2.1 Tool life study during Inconel DA 718 machining

Fig. 23 shows the evolution of tool life in relation to the length of cut data during the machining of an Inconel 718 DA alloy. The rate of flank wear was significantly greater in the samples deposited by CAE at different voltages (A30 and A150 V) compared to that of the coating deposited by HiPIMS. Experimental results have shown that tools coated by HiPIMS had substantially superior performance than those coated by CAE (1200 m vs. 500 m prior to flank wear failure). IN 718 DA machining usually undergoes heavy abrasion due to the presence of hard carbide particles in its structure [22]. The HiPIMS coating possessed higher hardness, better load support parameter (H^3/E^2) ratio and superior adhesion, which are critical for the machining of this type of material.

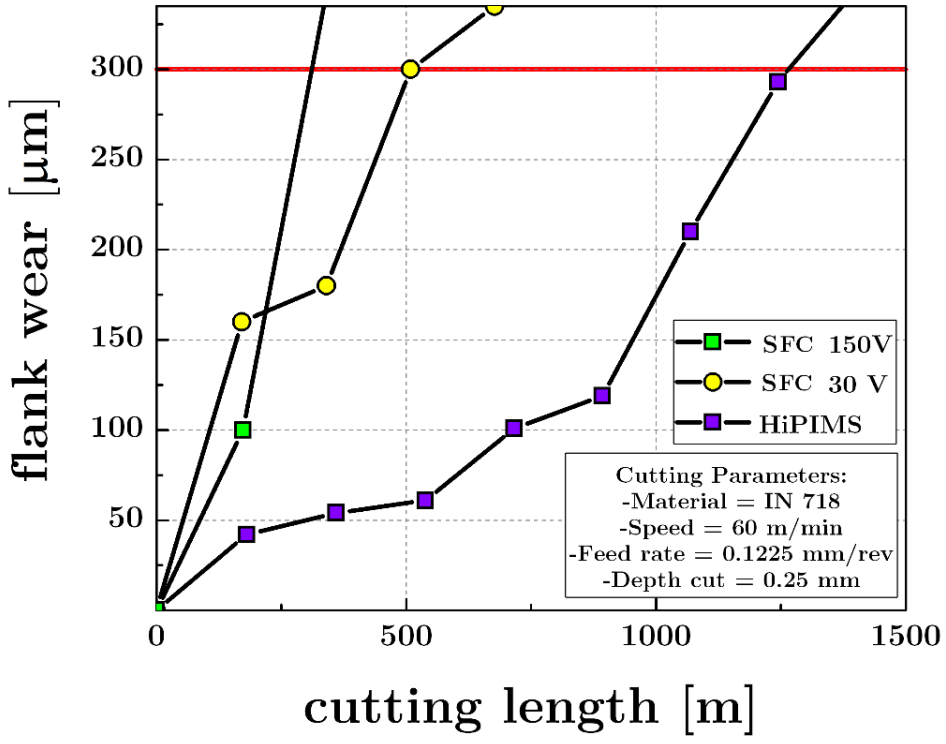

Figure 23 - Flank wear vs. length of cut during DA IN 718 machining

High temperatures and pressures within the cutting zone are typical under these conditions [23]. The coating layer was expected to inhibit heat transfer into the tool, which would keep the tool's temperature lower and thus and thus avoid reducing its mechanical strength while focusing heat into the workpiece thus raising its temperature and reducing its mechanical strength making it easier to machine.

Fig. 24 shows the graph of notch wear intensity plotted against the cutting length. The wear curve of tools with a HiPIMS coating consists of three typical stages: an initial running-in stage, a stable region, and a point after which rapid tool wear and failure occurs. Conversely, CAE coatings do not feature a steady state wear region, but instead directly proceed to failure.

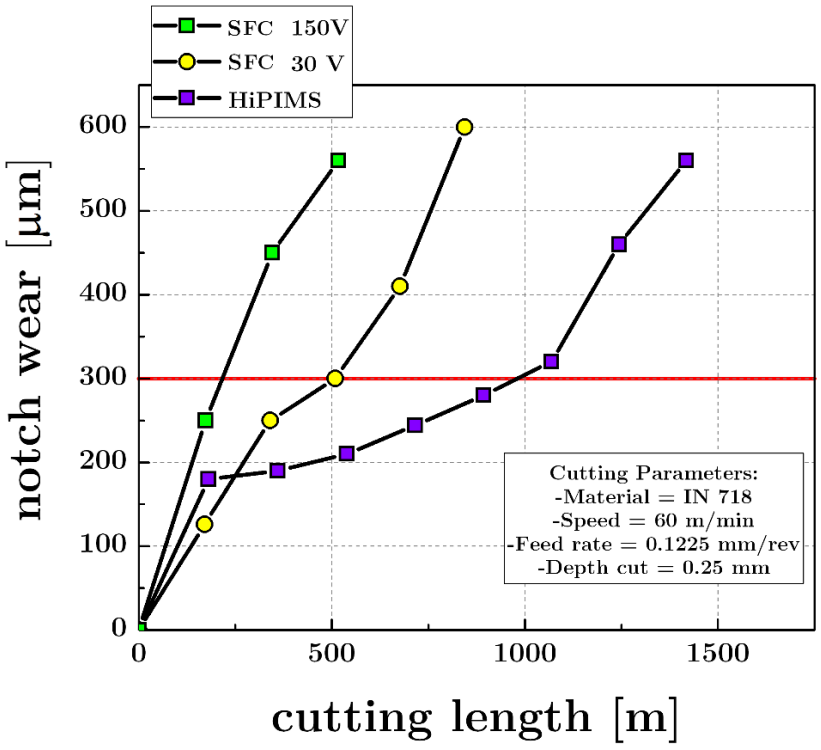

Figure 24 - Notch wear vs. length of cut during machining of DA IN 718.

The CAE coating deposited on the tool at a bias voltage of 150 V, undergoes coating delamination and subsequent rapid failure, as can be observed in Fig. 24. This behaviour can be associated with the brittleness of this coating as well as the point defects typical in the CAD process. Elevated plasma energy during deposition might propagate the concentration of defects. The CAE coating deposited at a bias voltage of 30 V featured intensive notch wear, which also resulted in rapid failure. However, in this instance, no delamination was observed to occur. Tool wear characteristics can be visualized in the following image (Fig. 25).

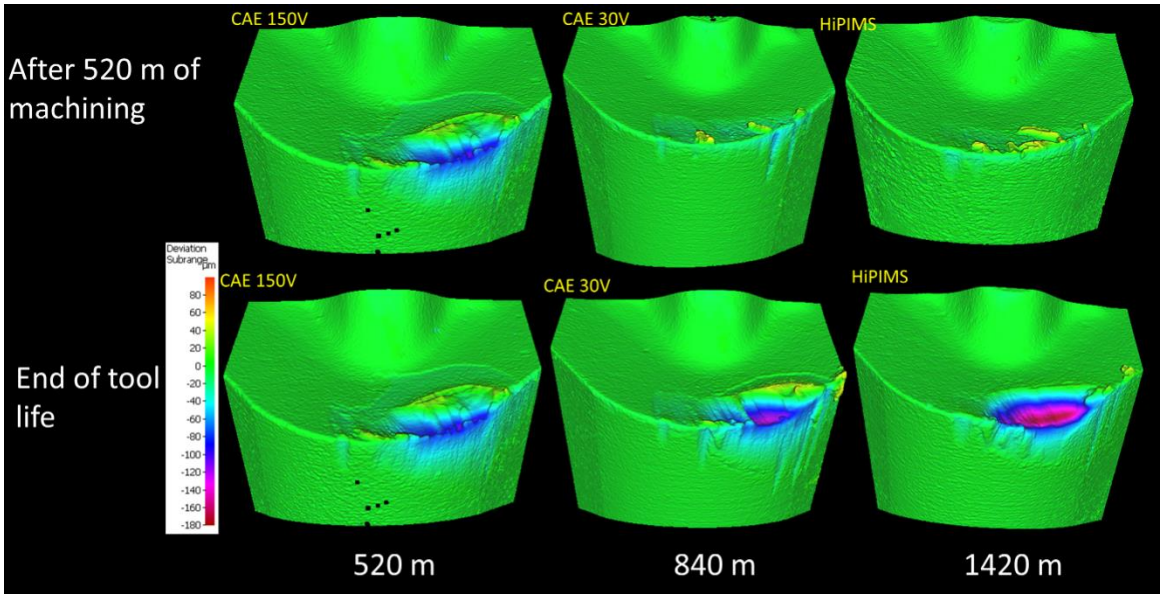

Figure 25 - 3D progressive tool wear stages that result after different lengths of cut.

The tool with a CAE coating deposited at a bias voltage of 150V rapidly reached wear failure due to the intensive delamination of the surface engineered layer. The noticeable presence of a BUE may have also resulted in poor coating performance. Abrasion marks on the flank surface were also visible due to the presence of hard carbide particles in the workpiece material, as was mentioned in previous chapters. In conclusion,

HiPIMS was shown to have improved the tool life to a greater degree than the CAE technique. One possible explanation for this, under the outlined cutting conditions, is the superior adhesion of this coating to the carbide substrate. In addition, the chip flow was facilitated by the formation of beneficial tribo-films as was discussed in previous chapters.

The material volumes removed from the rake face by the various coated tools studied, are plotted in Fig. 26. High temperatures observed during the machining of a DA Inconel 718 alloy cause diffusion between the tool and the workpiece, which results in crater wear. The data presented in Figure 31 are similar in performance to the flank wear data.

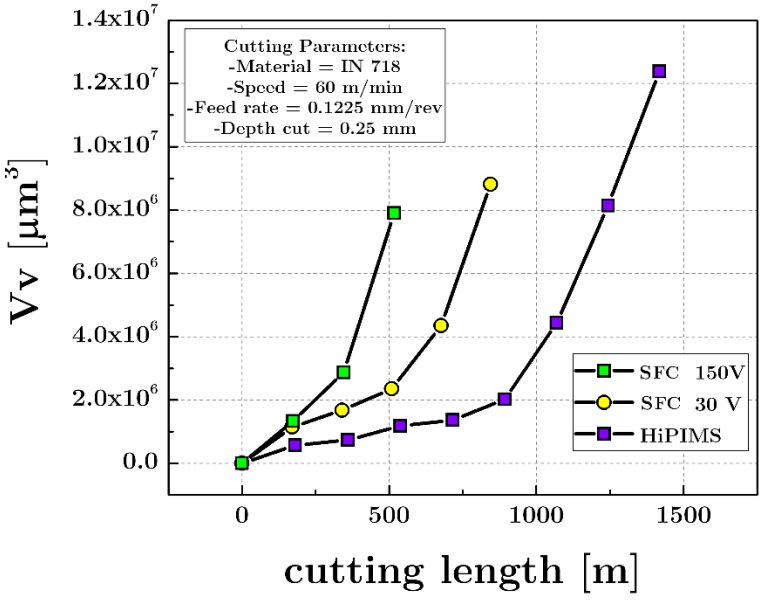

Figure 26 - Volume of material (Vv) below the original reference

The volumetric data of the region above the rake face of different cutting tools are presented in Fig. 27. During machining of Inconel DA 718 alloy, high cutting temperatures promote BUE formation. This is caused by the adhesion of workpiece material on the cutting tool edge. Since this method only measures volumes, the periodic adhesion of

workpiece material to the tip of the tool affects the measured volume of the peaks, as can be seen at the highest point in the graph of the SFC 150 V coating.

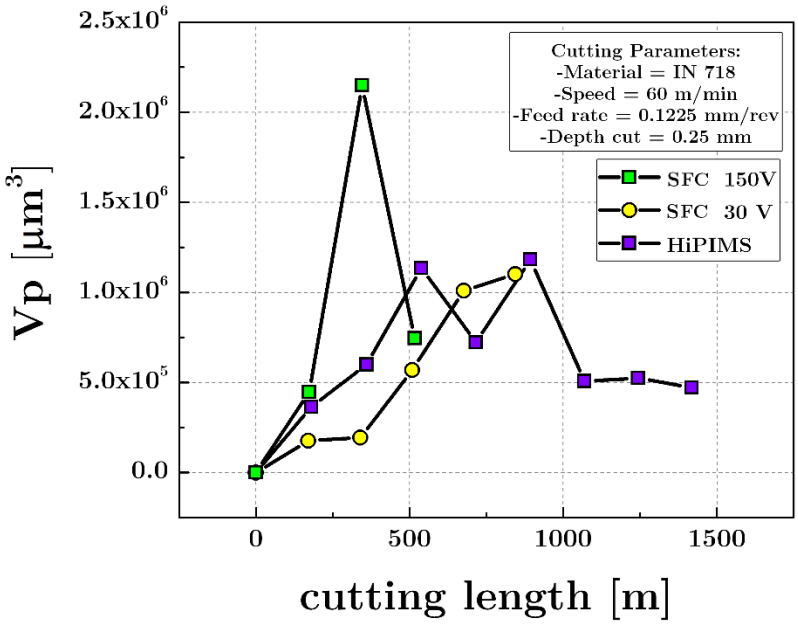

Figure 27 - Volumetric peaks above the reference.

Average forces after the first pass are shown in Fig. 28 for all analyzed coatings. Following three measurements for each coating, large fluctuations in the values of wear forces have been observed, with standard deviation ranging in the double digits. The obtained results did not show significant differences in force for all the studied coatings.

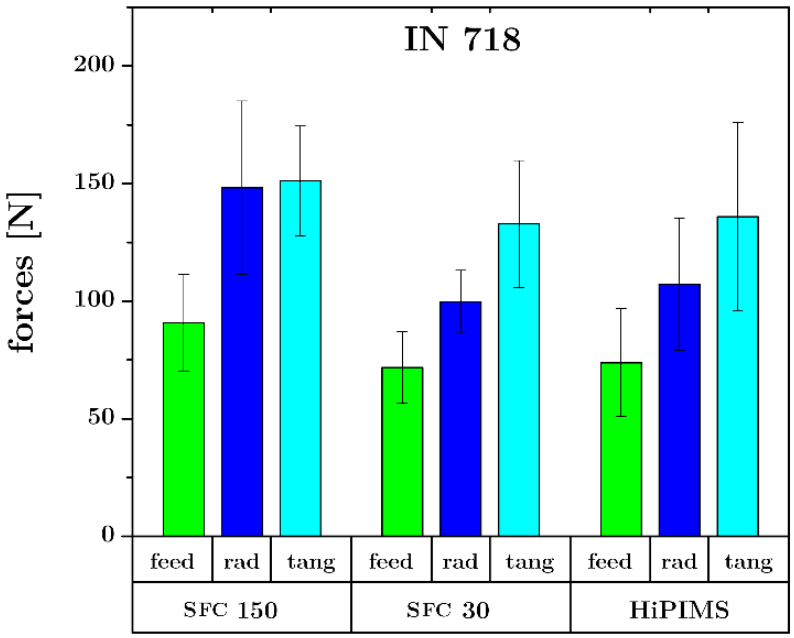

Figure 28 - Average cutting forces during machining of DA Inconel 718 alloy.

4.2.2 Tool life study on machining of SS 304

The machining of SS 304 does not involve hard carbide inclusions in the workpiece as nickel-based materials, instead, its high toughness and ductility leads to intensive sticking of workpiece material to the tip of the tool, known as adhesive wear that can result in BUE formation [24]. The high temperatures in the cutting zone also can reduce tool life, due to its poor thermal conductivity [25]. Fig. 29 shows the progression of flank wear against machining cutting length.

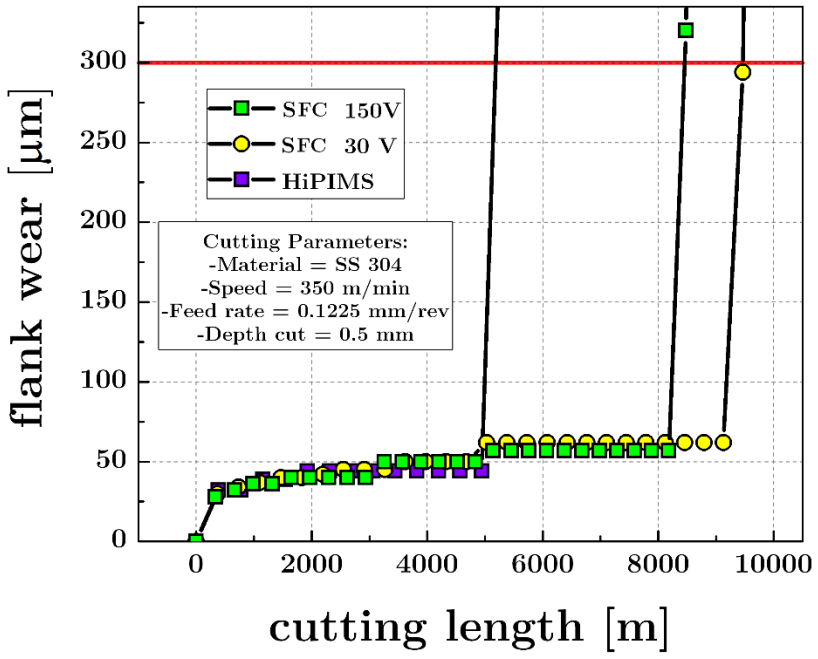

Figure 29 - Evolution of flank wear of machining experiment of SS 304.

The best performance in this experiment was reached by SFC 30V coated tool after machining 9400 m. HiPIMS reached failure at 4900 m which is almost 50% worse. This, performance difference was unexpected based on the IN718 results. In fact, the good features of HiPIMS coating mentioned for IN718 were not manifested in this experiment when compared to the SFC deposition technique. An in-depth investigation into the reasons for this behavior was performed and will be discussed in this chapter.

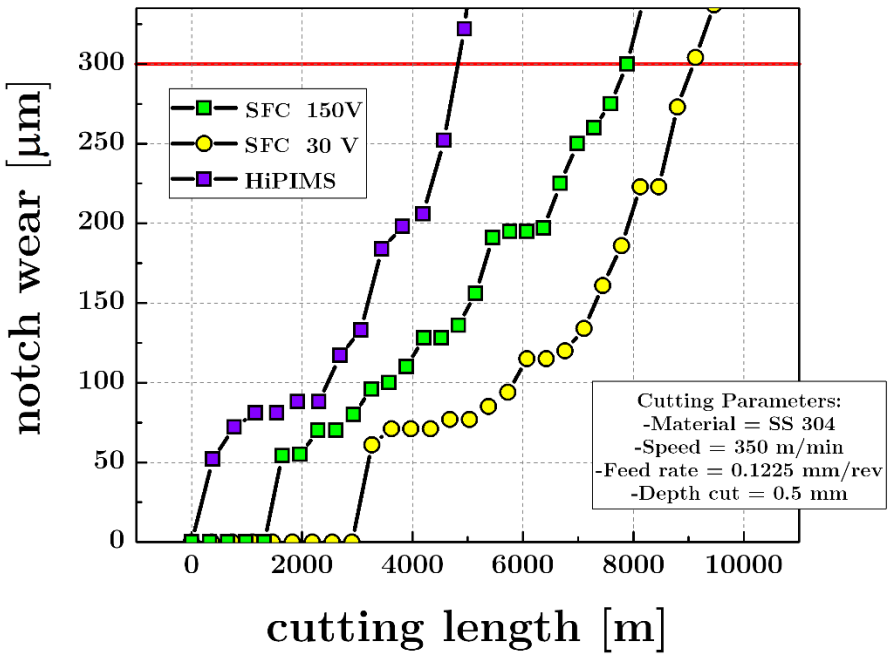

Figure 30 - Evolution of notch wear of machining experiment of SS 304.

In this experiment of machining of SS 304, flank wear had practically no variation during cutting, while notch wear grows gradually and significantly until failure (Fig. 30). A 3D volume comparison between the coatings in different cutting lengths are plotted in Fig. 31. Machining 304 with the HiPIMS coated tool presented higher amount of notch wear on the flank face combined with crater wear on the rake face than the CAE SFC coatings. For SFC 30 V sample (top right) a peak of BUE formation is noticeable located on top of where notch wear was located.

Fig. 32 shows the plotting of Volume of peaks (Vp), which is the measurement of amount of material adhered to the tool by 3D optical microscopy, against cutting length. Since the adhesion and BUE formation are subjected to high pressure, temperature, and friction, the amount of adhered materials presented on the tool are constantly varying. The SFC 150V tool presented a lot of adhered material since the first pass ($4 \times 10^6\ \mu m^3$), with subsequent oscillation in its thickness occurring until failure.

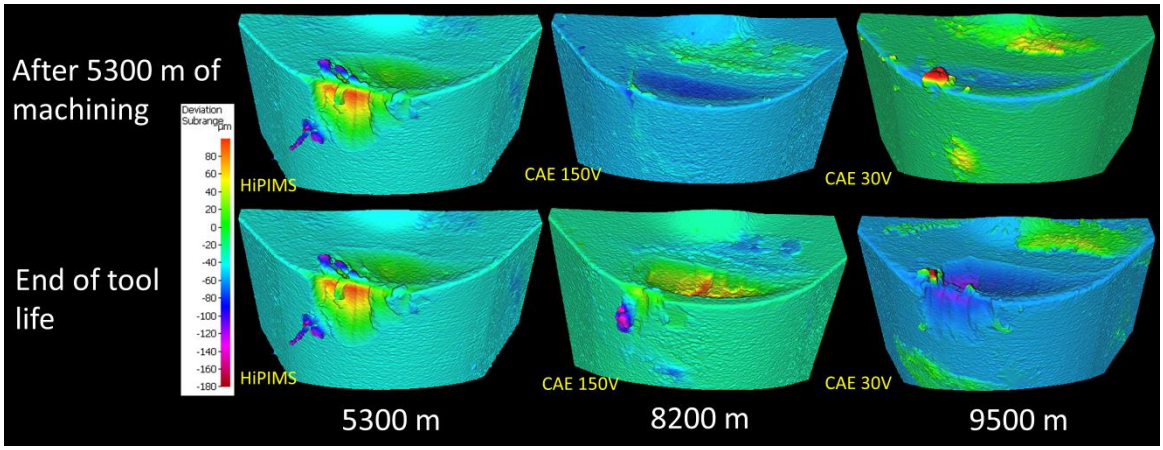

Figure 31 - 3D comparative coating evaluation by Alicona microscope.

The Vp results shown in Fig. 32 present a gradual increase with removed material, with HiPIMS reaching failure first. In Fig. 33 the Volume of valleys (Vv), which is the measured amount of material that is removed from the tool, is plotted against cutting length. In both cases SFC outperforms HiPIMS.

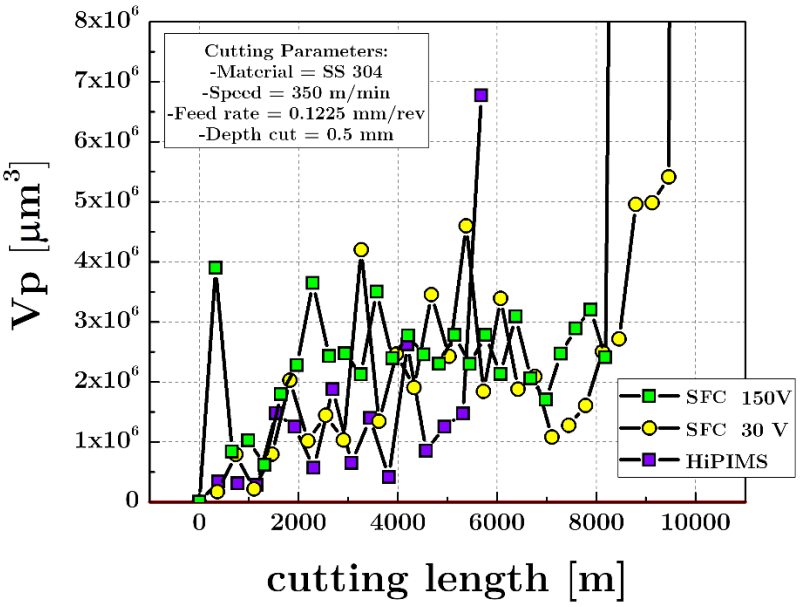

Figure 32 - Volume of peaks (Vp) above the original reference on different cutting lengths

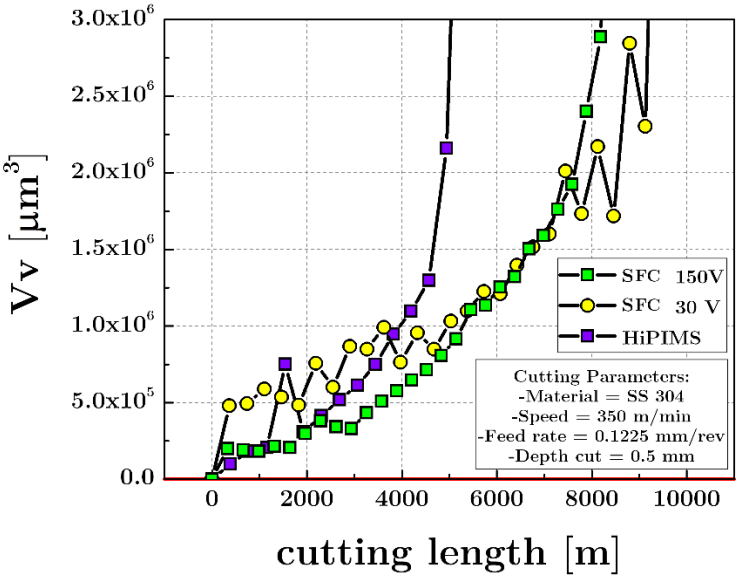

Figure 33 - Volume of valleys (Vv), material below the original reference on different cutting lengths.

Forces measurement of first pass of cutting is plotted in Fig. 34. No differences were found in forces between the coatings the considering the level of deviation in the

measured values. This shows no net improvement in cutting force with the better properties associated with the HiPIMS coating.

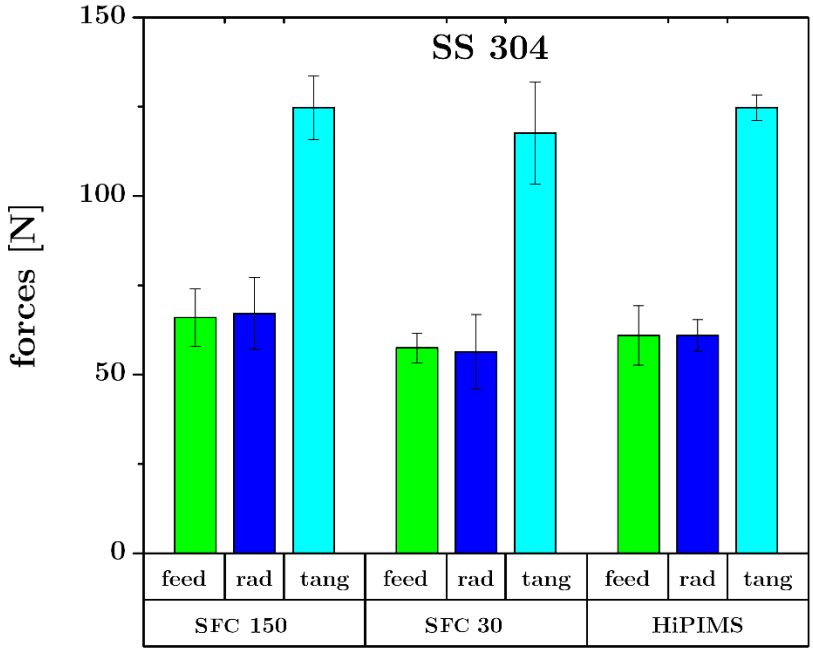

Figure 34 - Average cutting forces of machining SS 304 by different coatings.

4.2.3 Wear pattern analysis of cutting tools on machining of IN 718 DA

Fig. 35 show the tool tip condition after one step of machining IN DA718 for two coatings. SFC coating presented a strong buildup formation combined with intensive crater wear, while HiPIMS presented lower wear.

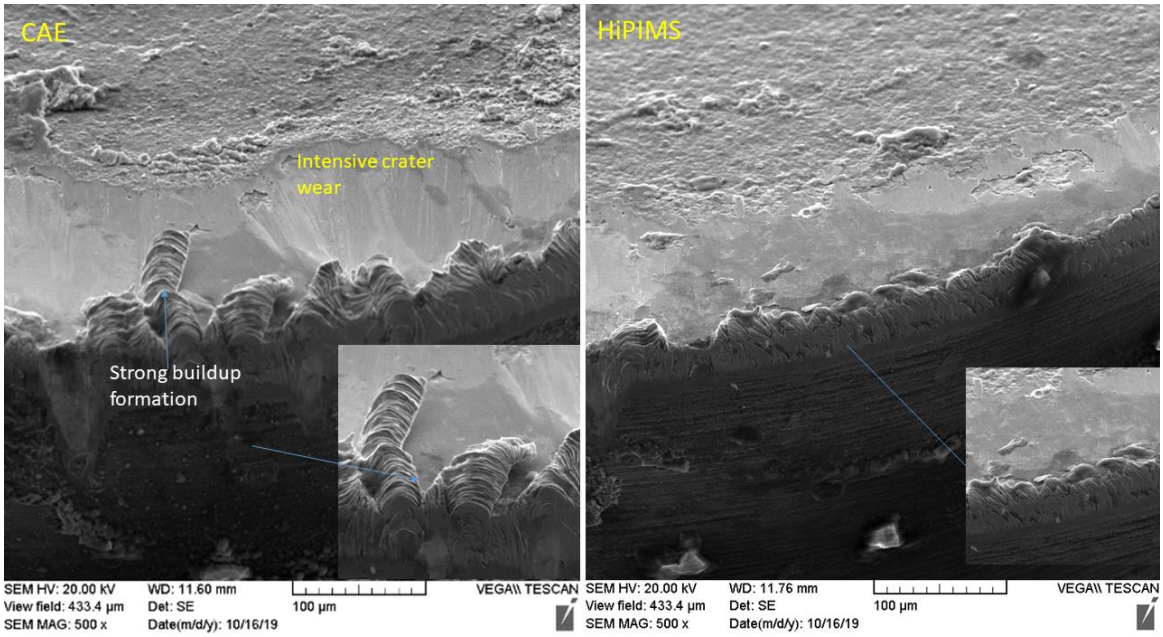

Figure 35 - SEM of cutting tools tip after cutting one pass of IN 718 DA.

Fig. 36 provides an overview of the critical region of the tool wear morphology obtained from machining of IN 718 DA at the same cutting length of 450 meters for both coatings. This analysis seeks to provide a detailed investigation of the tool wear patterns that resulted from Study B.

The machining of nickel-based materials [26], [27] is known for its intense mechanical and thermal fatigue loading, which results in failure (wear patterns) on the cutting tools such as notching at the depth of cut region primarily, as well as flank and crater wear. The low thermal conductivity of Inconel leads to high temperatures in the cutting zone, followed by BUE formation. The main two wear mechanisms involved are oxidation and abrasion, resulting in an unstable attrition wear mode [28].

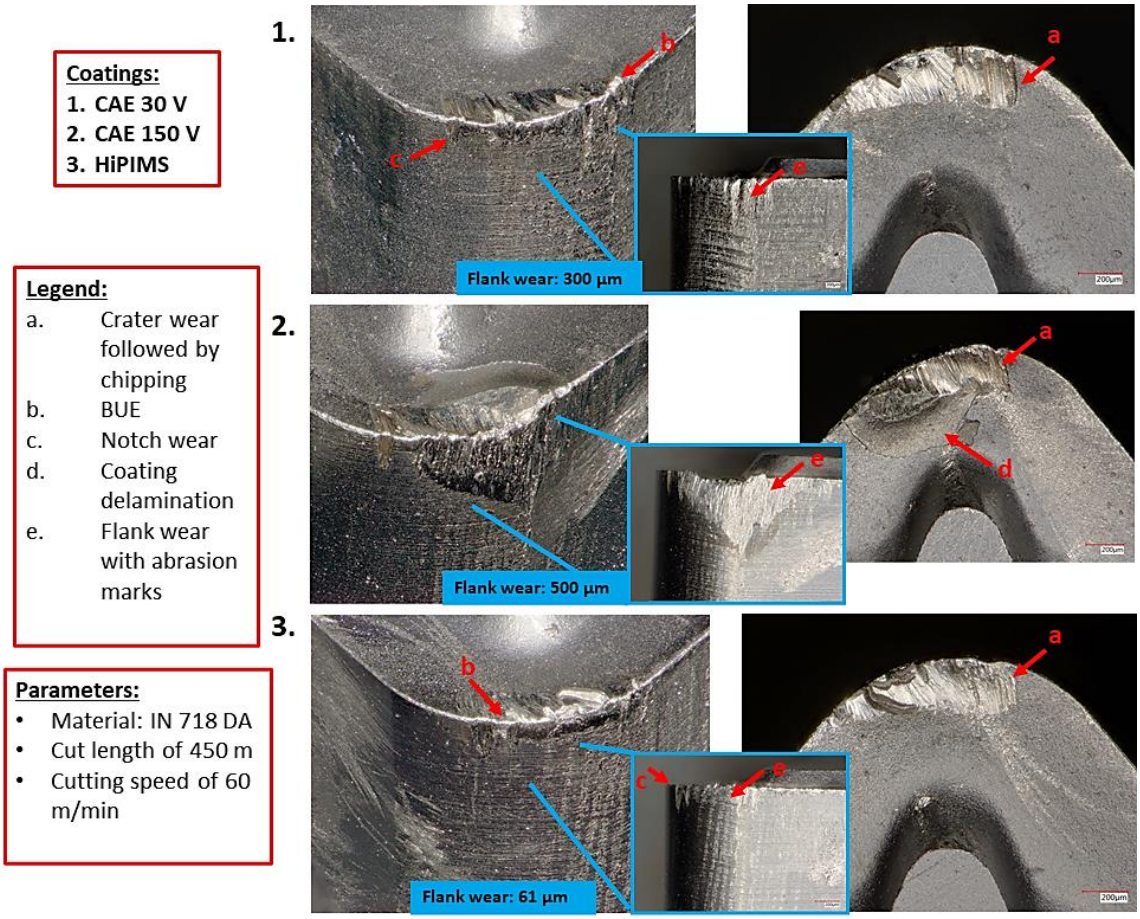

Figure 36 - 3D Optical microscopies indicating main wear patterns on machining of IN DA718.

4.2.4 Microscopy of cutting tools on machining of SS 304

A summary of important factors that are present during machining of Stainless Steels can be summarized as follows:

1. Martensitic transformation by the presence of high work hardening [25].
2. Low thermal conductivity, which can restrict heat flow resulting in high temperatures in the cutting zone [29], [30].
3. High ductility and toughness, which can lead to high levels of BUE formation [25].
4. High cutting forces which necessitate rigid tooling to overcome chatter.

5. Burr formation at the end of the depth of cut, which produces hardened material that can remove the coating layer resulting in notch wear [29].

Fig. 37 shows 3D microscopy images showing the wear patterns of machining of SS 304. Notch wear and crater wear were the main pattern found in this experiment. Higher notch wear, 322 microns, was observed when machining with the HiPIMS deposited coating for a cutting length of 5000 meters, while SFC 30V was observed to have 77 microns of wear.

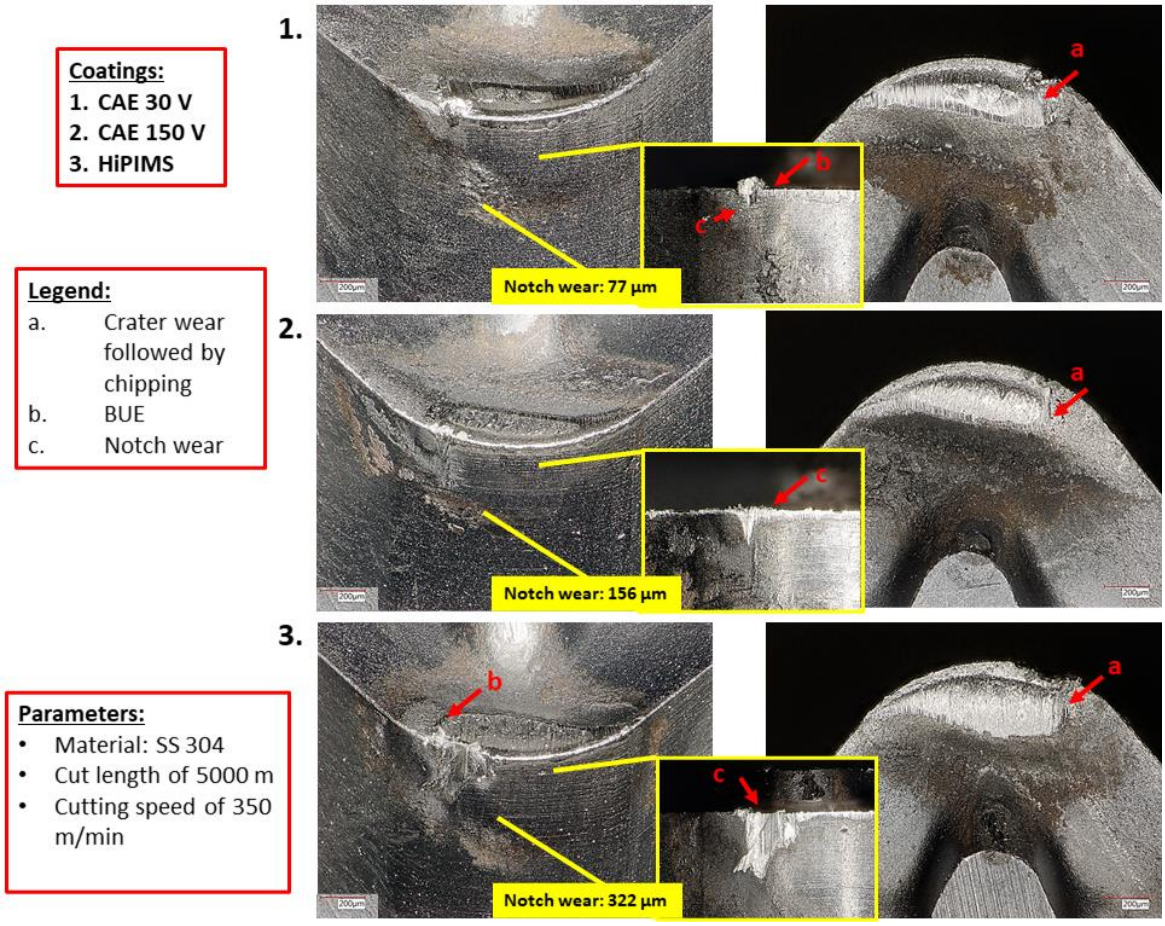

Figure 37 - 3D Optical microscopies indicating main wear patterns on machining of SS 304.

4.2.5 Chip analysis

The analysis of the chip segmentation can offer a clear indication of the general condition in machining and tool wear. Moreover, strong correlations between the mechanism of chip formation to forces that are present in the process can arise from these studies [31]. Basic definitions that were used in this study will be presented next.

Segmentation ratio (SR) was used. It is an indication of the maximum chip thickness H_{max} [32].

$$SR = \frac{H_{max} - H_{min}}{H_{max}}$$

The equivalent chip thickness (H_{eq}) in chip analysis can be calculated as follows.

$$H_{Eq} = H_{max} + \frac{H_{max} - H_{min}}{2}$$

The chip compression ratio (*CCR*), as stated by Shaw et al., is the ratio of the uncut chip thickness (t) to the chip thickness (t_c) [12].

$$CCR = \frac{t}{t_c}$$

For a turning operation, the uncut chip thickness can be calculated by using the feed rate (f) and rake angle (α) as follows.

$$t = f \times \cos\alpha$$

The shear angle can be determined using the following formula.

$$\tan\phi = \frac{r\cos\alpha}{1 - r\sin\alpha}$$

Shear strain is defined as:

$$\gamma = \frac{\cos\alpha}{\sin\phi\cos(\phi - \alpha)}$$

Chip velocity can be calculated as follows.

$$V_C = \frac{\sin \phi}{\cos (\phi - \alpha)} V$$

The measurements of chip thickness and results from the chip analysis are plotted in Table 8. Coatings that performed better during machining presented lower thicknesses than others, HiPIMS on IN DA718 and SFC 30V on SS 304. This is related to the amount of plastic deformation of the material during cutting, with shear strain being the quantification variable. For the case machining of SS 304where HiPIMS performed worse than SFC, its shear strain is around 40% higher, indicating that high work hardening was present. Chip sliding velocity V_C, was shown to be higher for coatings that performed better. This can indicate that if the shearing process requires lower energy, with lower energy being used to generate heat, more energy will be converted to momentum, allowing higher chip velocities. Researchers [25] already reported the high ductility of austenitic stainless steel, in which transformation to martensitic structures by the high temperatures in cutting zone that can reach temperatures up to 1200°C [33]. At such high temperatures, degradation of AlTiN coatings can occur. Studies showed that the inclusion of Cr in the coating, which can support high temperatures up to 1100°C with subsequence presence of dense $\alpha(Al, Cr)_2O_3$ mixed oxides, can enhance adhesion and the tool life of HiPIMS coatings in comparison to AlTiN [33], [34].

Table 8 - Chip characterization

Coating	t_c, mm	H_{Eq}, mm	CCR	SR	ϕ (°)	γ	V_C, m/min
IN 718							
SFC 30	0.153	0.172	0.78	0.25	52.43	1.62	62.5
SFC 150	0.173	0.179	0.69	0.61	45.35	1.65	51.1
HiPIMS	0.138	0.179	0.87	0.23	59.38	1.68	76.3
SS 304							
SFC 30	0.249	0.319	0.48	0.57	29.97	2.06	183.8
SFC 150	0.270	0.356	0.44	0.63	27.40	2.20	167.1
HiPIMS	0.365	0.482	0.33	0.64	19.75	2.92	119.3

The hardness results of the chips are presented in Table 9. Accordingly, when considering observations of shear strain, an increase in hardness was also attributed to induced strain in the material [28]. The increased chip hardness (6.08 GPa) of SFC 30V sample on machining of IN DA718 means that more energy must be employed to promote strain, in comparison to HiPIMS (5.34 GPa).

Table 9 - Chip hardness. (*indicates the best tool)

Coating	W/P Hardness (GPa)	Chip Hardness (±0.3 GPa)
IN 718	1.138	
SFC 30		6.08
SFC 150		5.43
HiPIMS*		5.34
SS 304	0.660	
SFC 30*		3.89
SFC 150		4.25
HiPIMS		4.45

4.2.6 SEM of chips

Fig. 38 shows SEM side view images of chips after one machining pass of IN DA718. The formation of large serrations on the chip edges relate to high strain values associated with chip formation during cutting. The HiPIMS chips presented smaller visual serration than others, indicating that less strain hardening was present during cutting, which also indicated better cutting performance with HiPIMS.

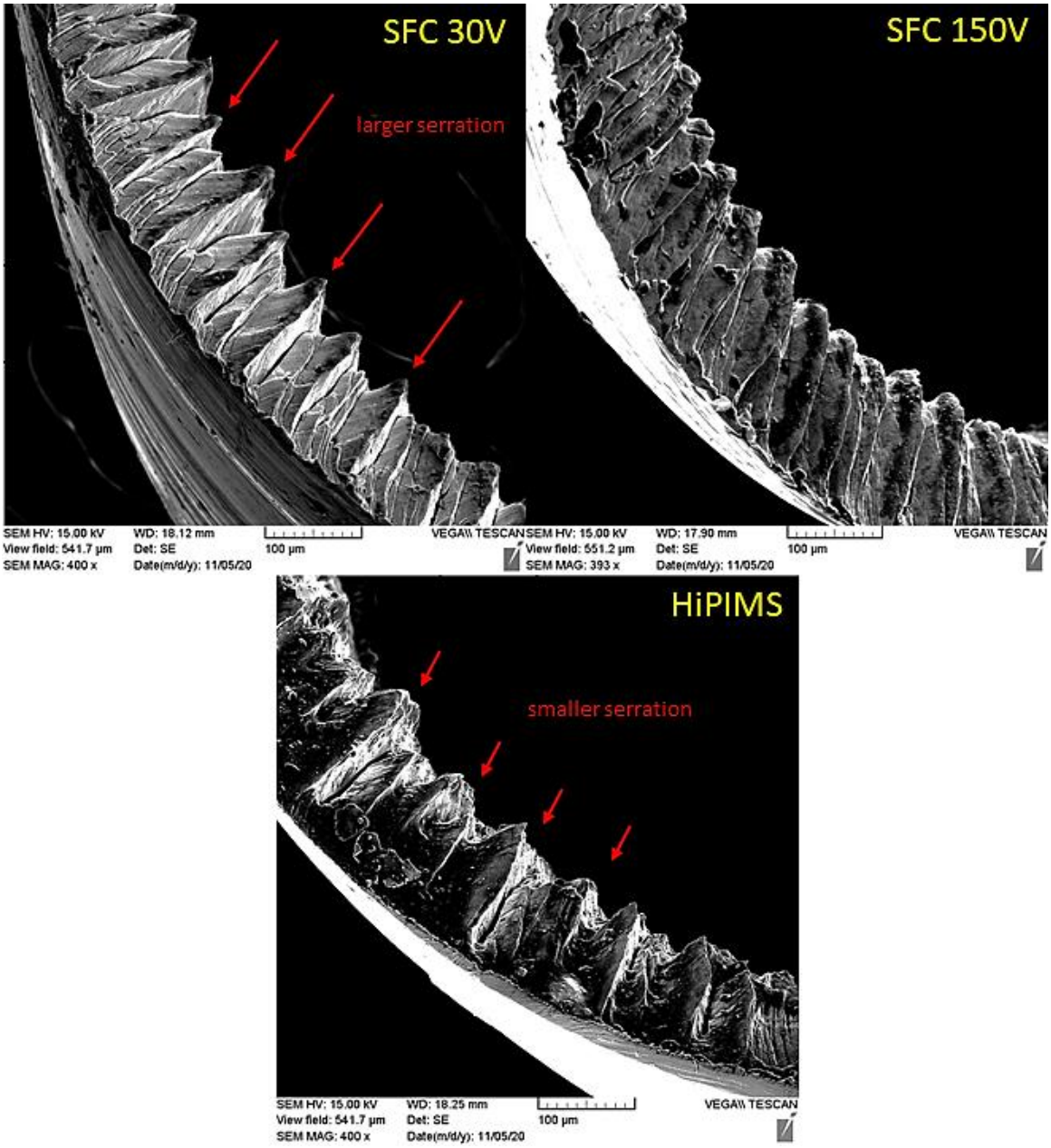

Figure 38 - SEM of IN 718 chips of study B.

SEM of tool/chip interface surface on machining of IN DA718 is shown in Fig. 39. A smoother surface was generated by the HiPIMS deposited coating, while SFC show abrasion marks originating at the hard inclusion points.

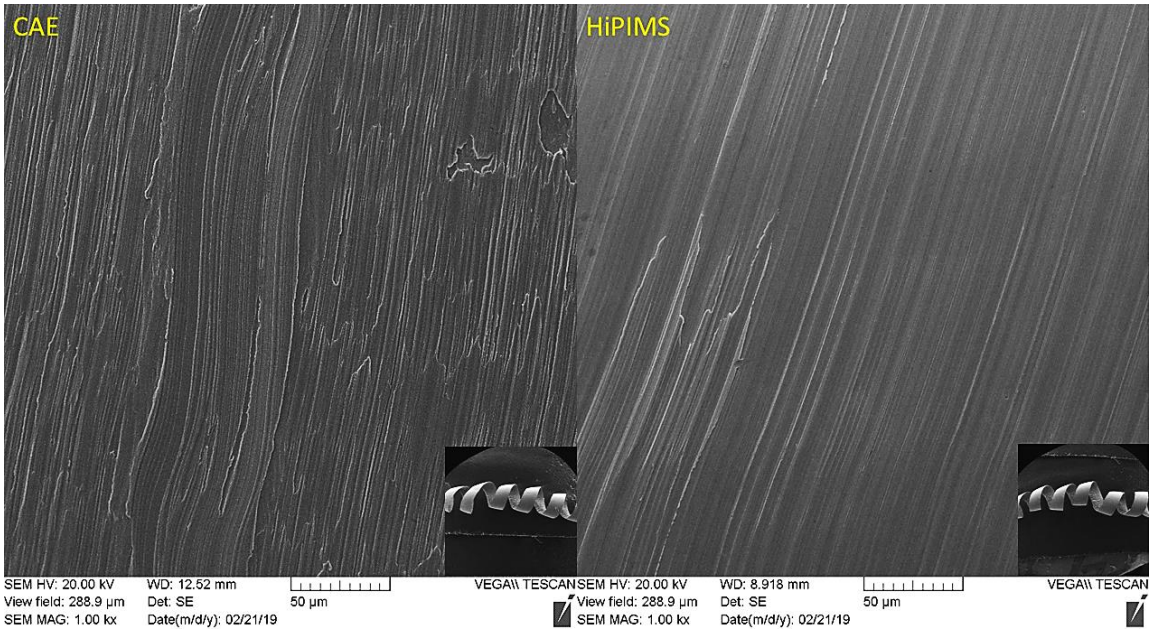

Figure 39 - SEM of tool/chip interface surface of machining of IN DA718.

Fig. 40 shows SEM side view images of chips after one SS 304 machining pass with slip planes indicated by red lines. The HiPIMS coating presents irregularities and not defined planes, while SFC coatings presents more homogeneous shearing planes. HiPIMS chips showed irregular shapes occurring within the chips, while SFC presented as more homogeneous deformation indicating better cutting conditions.

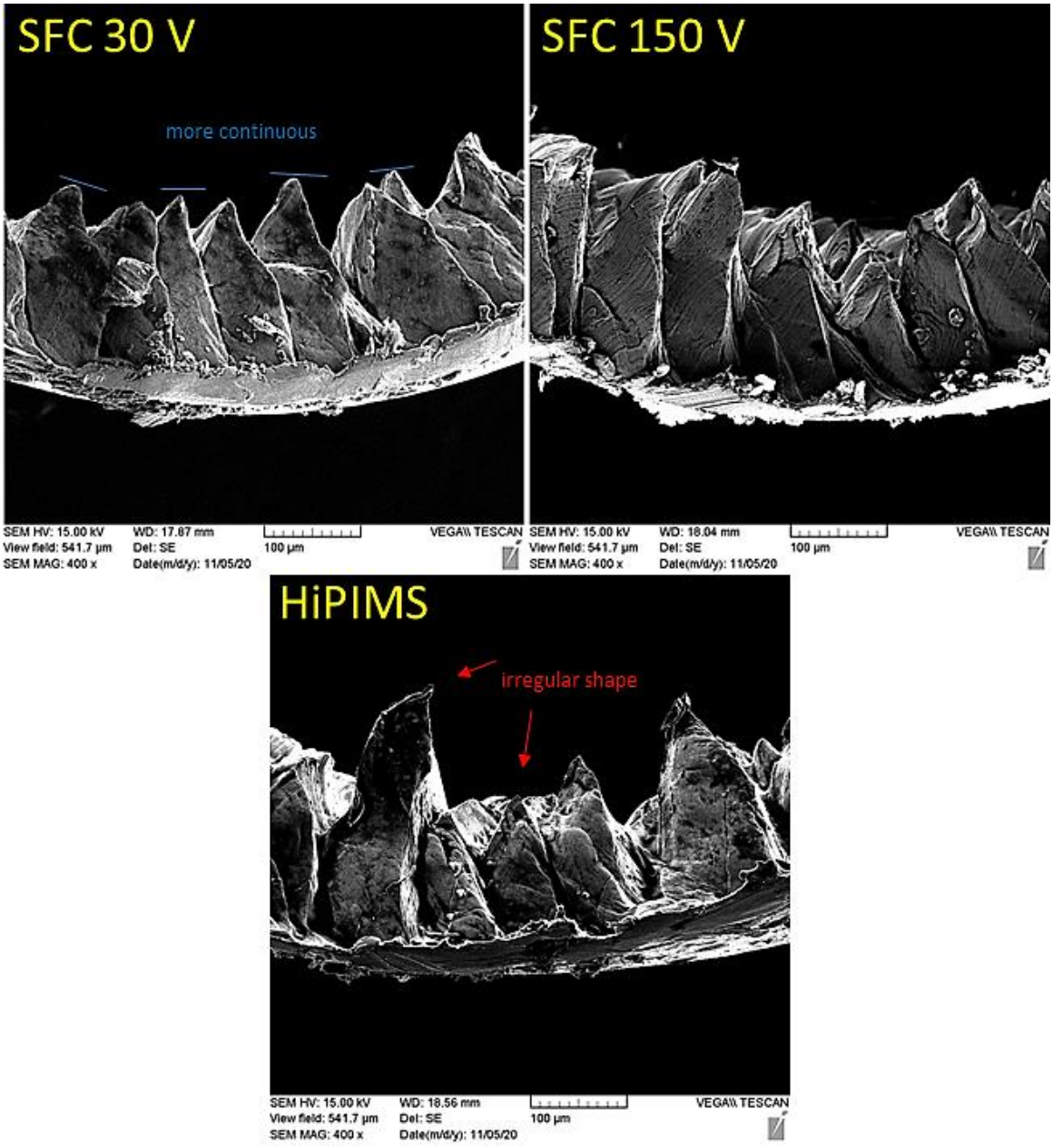

Figure 40 - SEM of SS 304 chips of study B.

4.2.7 Final considerations

Tools with HiPIMS deposited coatings demonstrated superior mechanical and physical properties during machining of Inconel 718 compared with the tools coated by the CAE deposition method. However, the converse was true when machining austenitic stainless steel using these coatings. One possible explanation for this discrepancy could be related to the frictional conditions at the tool/workpiece interface.

Fox-Rabinovich et al. [35] described two categories of tribo-films which are produced through the frictional process. The first type is super-ductile and represents lubricating films generated by structural activation during friction, which lead to an increase of energy dissipation. The ductility of these oxides can provide lubrication, whereas their resistance to breakdown under high temperatures can help protect the tool substrate from the heat generated within the cutting zone. The second type is characterized by supersaturated compounds that are thermally activated and feature insulating thermal properties combined with high temperature hardness and strength [35].

Since the SS 304 machining experiment was performed at a relatively high speed (350 m/min) with possible martensitic phase formation, the temperatures in the cutting zone can exceed 1100°C [25], [30]. Chemical stability also plays an important role, since different workpiece alloying elements can yield different results. Shear strain data and chips analysis showed that the chips formed by the CAE 30V coating are 15% softer than those of HiPIMS. This means that the HiPIMS coated tool requires a greater amount of energy to cut the same material under the same conditions, generating higher plastic deformation and heat. This can be attributed to the degradation of alumina tribofilms at the high

temperatures associated with machining. AlTiN coatings were reported to be capable of sustaining temperatures of up to about 800°C, whereas chromium based coatings such as AlTiCrN where reported to sustain temperatures up to 1100 °C and improve tool life during cutting of austenitic stainless steel [36]. Tool patterns also showed intensive crater and notch wear, which is an indicative of intensive heat generation in the secondary deformation zone as defined by the classical orthogonal model. Notch wear specifically can be related to the high shear strain during cutting of stainless steel, which could be observed by the chip formation.

4.2.8 Conclusions of Study B

- The PVD coating deposited by the HiPIMS method exhibited a longer tool life during the machining of Inconel DA 718 and a reduced tool life during the machining of SS 304 in comparison with the CAE applied coatings
- Lower thicknesses, shear strain and hardness were found in chips produced by the best performing tools, indicating an optimal combination of shearing and frictional characteristics during cutting.

CHAPTER 5 – GENERAL CONCLUSIONS

The general conclusions of this research are the following:

- The surface morphology of coatings deposited by HiPIMS was smoother than that of CAE, mainly due to the formation of droplets during deposition.
- HiPIMS produces a higher amount of sapphire tribo-films during operation than CAE.
- HiPIMS exhibited lower values of compressive residual stress than CAE.
- Coating adhesion and density were superior with HIPIMS compared with CAE Inconel 718 machining. This had a direct impact on tool life.
- HiPIMS performed poorly compared to CAE during the machining of Stainless Steel 304. High speeds, temperatures and strains generated during cutting led to faster wear progression, despite the coating's enhanced mechanical and physical properties. A higher amount of sapphire tribofilms on the surface of the HiPIMS coated tool was found to not help improve tool life due to their tendency to become detached under the outlined cutting conditions.

CHAPTER 6 – SUGGESTIONS FOR FUTURE WORK

Suggestions for further studies related to this work are presented as follows:

- A coating optimization study involving the tuning of HiPIMS coating parameters can be done by comparing different parameters of deposition to machining performance.
- The machining of stainless steel presented a complex machining behaviour that is not completely understandable. Additional advanced machining studies are required to better understand the demands placed on the coating. Temperature in the cutting zone seems to be a key information for better understanding. Thermal imaging is a fast method that can be applied in future studies.

REFERENCES

[1] D. M. Mattox, *Handbook of physical vapor deposition (PVD) processing.* William Andrew, 2009.

[2] K. S. Sree Harsha, *Principles of Vapor Deposition of Thin Films*. Elsevier, 2006.

[3] K. D. Bouzakis, N. Michailidis, G. Skordaris, E. Bouzakis, D. Biermann, and R. M'Saoubi, "Cutting with coated tools: Coating technologies, characterization methods and performance optimization," *CIRP Ann. - Manuf. Technol.*, 2012.

[4] B. Chapman, *Glow discharge processes: sputtering and plasma etching.* Wiley, 1980.

[5] P. H. Mayrhofer, C. Mitterer, L. Hultman, and H. Clemens, "Microstructural design of hard coatings," *Prog. Mater. Sci.*, vol. 51, no. 8, pp. 1032–1114, 2006.

[6] Q. Luo, S. Yang, and K. E. Cooke, "Hybrid HIPIMS and DC magnetron sputtering deposition of TiN coatings: Deposition rate, structure and tribological properties," *Surf. Coatings Technol.*, 2013.

[7] P. Kulkarni, A. Marsan, and D. Dutta, "A review of process planning techniques in layered manufacturing," *Rapid Prototyp. J.*, vol. 6, no. 1, pp. 18–35, 2000.

[8] M. Bilokur, A. R. Gentle, M. D. Arnold, M. B. Cortie, and G. B. Smith, "High temperature optically stable spectrally-selective Ti1-xAlxN-based multilayer coating for concentrated solar thermal applications," *Sol. Energy Mater. Sol. Cells*, 2019.

[9] T. J. Morton, "Development of High Temperature-Oxidation Resistant PVD Coatings for Cutting Tools Using HIPIMS," no. October, 2016.

[10] P. M. Martin, *Deposition technologies for films and coatings*. 2005.

[11] U. Helmersson, M. Lattemann, J. Bohlmark, A. P. Ehiasarian, and J. T. Gudmundsson, "Ionized physical vapor deposition (IPVD): A review of technology and applications," *Thin Solid Films*. 2006.

[12] Miltion C. Shaw, *Metal cutting principles (Second edition)*, vol. 7. 2005.

[13] F. Klocke and T. Krieg, "Coated tools for metal cutting - features and applications," *CIRP Ann. - Manuf. Technol.*, vol. 48, no. 2, pp. 515–525, 1999.

[14] H. Takaoka, E. Nakamura, T. Oshika, and A. Nishiyama, "Relationship between an affinity of (Ti1-x, Alx)N layer toward iron and its cutting performance," *Surf. Coatings Technol.*, vol. 177–178, pp. 306–311, 2004.

[15] A. Inspektor and P. A. Salvador, "Architecture of PVD coatings for metalcutting applications: A review," *Surf. Coatings Technol.*, vol. 257, pp. 138–153, 2014.

[16] I. J. R. Baumvol, F. C. Stedile, W. H. Schreiner, F. L. Freire Jr, and A. Schröer, "Deposition and characterization of non-conducting silicon nitride, aluminum nitride and titanium-aluminum nitride thin films," *Surf. Coatings Technol.*, vol. 59, no. 1–3, pp. 187–192, 1993.

[17] P. Villars, A. Prince, H. Okamoto, and others, *Handbook of ternary alloy phase diagrams*, vol. 5. ASM international Materials Park, OH, 1995.

[18] H. Elmkhah, T. F. Zhang, A. Abdollah-zadeh, K. H. Kim, and F. Mahboubi, "Surface characteristics for the Ti Al N coatings deposited by high power impulse magnetron sputtering technique at the different bias voltages," *J. Alloys Compd.*, vol. 688, pp. 820–827, Dec. 2016.

[19] K. Persson and M. Project, “Materials Data on TiN by Materials Project.”

[20] V. D. Mote, Y. Purushotham, and B. N. Dole, “Williamson-Hall analysis in estimation of lattice strain in nanometer-sized ZnO particles,” pp. 2–9, 2012.

[21] J. M. F. de Paiva *et al.*, “Frictional and wear performance of hard coatings during machining of superduplex stainless steel,” *Int. J. Adv. Manuf. Technol.*, vol. 92, no. 1–4, pp. 423–432, 2017.

[22] A. Marques, M. Paipa Suarez, W. Falco Sales, and Á. Rocha Machado, “Turning of Inconel 718 with whisker-reinforced ceramic tools applying vegetable-based cutting fluid mixed with solid lubricants by MQL,” *J. Mater. Process. Technol.*, 2019.

[23] S. Roy, R. Kumar, Anurag, A. Panda, and R. K. Das, “A brief review on machining of inconel 718,” in *Materials Today: Proceedings*, 2018.

[24] F. B. Pickering, “Metal cutting,” *Int. Met. Rev.*, vol. 23, no. 1, pp. 202–203, 2014.

[25] M. Kaladhar, K. Venkata Subbaiah, and C. H. Srinivasa Rao, “Machining of austenitic stainless steels - A review,” *Int. J. Mach. Mach. Mater.*, vol. 12, no. 1–2, pp. 178–192, 2012.

[26] E. O. Ezugwu, Z. M. Wang, and A. R. Machado, “The machinability of nickel-based alloys: A review,” *J. Mater. Process. Technol.*, vol. 86, no. 1–3, pp. 1–16, 1998.

[27] D. Zhu, X. Zhang, and H. Ding, “Tool wear characteristics in machining of nickel-based superalloys,” *International Journal of Machine Tools and Manufacture*. 2013.

[28] S. Capasso *et al.*, “A novel method of assessing and predicting coated cutting tool wear during Inconel DA 718 turning,” *Wear*, vol. 432–433, no. June, p. 202949, 2019.

[29] A. E. Diniz, Á. R. Machado, and J. G. Corrêa, "Tool wear mechanisms in the machining of steels and stainless steels," *Int. J. Adv. Manuf. Technol.*, vol. 87, no. 9–12, pp. 3157–3168, 2016.

[30] R. M'Saoubi, J. C. Outeiro, B. Changeux, J. L. Lebrun, and A. Morão Dias, "Residual stress analysis in orthogonal machining of standard and resulfurized AISI 316L steels," *J. Mater. Process. Technol.*, vol. 96, no. 1–3, pp. 225–233, 1999.

[31] A. Antić, P. B. Petrović, M. Zeljković, B. Kosec, and J. Hodolič, "The influence of tool wear on the chip-forming mechanism and tool vibrations," *Mater. Tehnol.*, vol. 46, no. 3, pp. 279–285, 2012.

[32] A. K. Parida, "Analysis of Chip Geometry in Hot Machining of Inconel 718 Alloy," *Iran. J. Sci. Technol. - Trans. Mech. Eng.*, vol. 43, no. s1, pp. 155–164, 2019.

[33] A. P. Kulkarni and V. G. Sargade, "Characterization and performance of AlTiN, AlTiCrN, TiN/TiAlN PVD coated carbide tools while turning SS 304," *Mater. Manuf. Process.*, vol. 30, no. 6, pp. 748–755, 2015.

[34] W. Kalss, A. Reiter, V. Derflinger, C. Gey, and J. L. Endrino, "Modern coatings in high performance cutting applications," *Int. J. Refract. Met. Hard Mater.*, vol. 24, no. 5, pp. 399–404, 2006.

[35] G. S. Fox-Rabinovich, I. Gershman, M. A. El Hakim, M. A. Shalaby, J. E. Krzanowski, and S. C. Veldhuis, "Tribofilm formation as a result of complex interaction at the tool/chip interface during cutting," *Lubricants*, vol. 2, no. 3, pp. 113–123, 2014.

[36] A. P. Kulkarni, G. G. Joshi, and V. G. Sargade, "Performance of PVD AlTiCrN

coating during machining of austenitic stainless steel," *Surf. Eng.*, vol. 29, no. 5, pp. 402–407, 2013.

APPENDIX

The average value of five measurements of each cutting tool from Study B are shown in Fig. 41. In this experiment, A30 and A150 (SFC CAE) performed better than HiPIMS during machining of SS and the opposite for IN. SFC coatings is also known for property of residual stresses near to zero, which can contribute to coating's integrity near the cutting edge. Since forces, as reported in Chapter 4.2, did not present to differ much for first pass, the edge radius differences then are not likely to produce significant impact of cutting process. Also, the fact that HiPIMS tools presented results between the other coatings and showed different tool life performances, contribute to the mentioned conclusions.

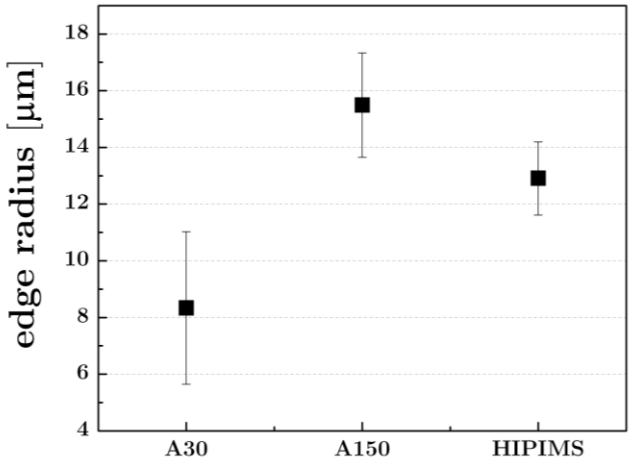

Figure 41 - Edge radius of cutting tools used for study B.

Fig. 42 shows the variation of coatings hardness, in crescent order, of different coatings measurements. Considering the measured values, few differences were found between coatings hardness, with exception of A30 (SFC) coating. Since SFC coatings provides coatings low residual stresses, hardness is slightly reduced.

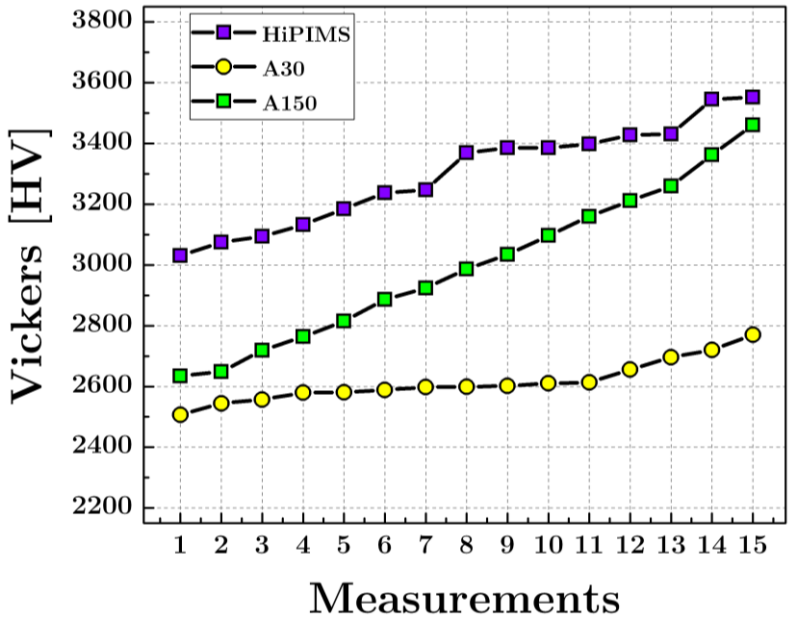

Figure 42 - Measurements of different coatings, by crescent order.

Fig. 43 shows side view and an overview of chips from machining of Inconel in study A. Side view of the chip shows smaller spacing of slip planes for HiPIMS tool in comparison to CAE which presented larger serration and spacing. HiPIMS coated tools performed better in this case, with better tool chip interaction produced by its enhanced coating properties.

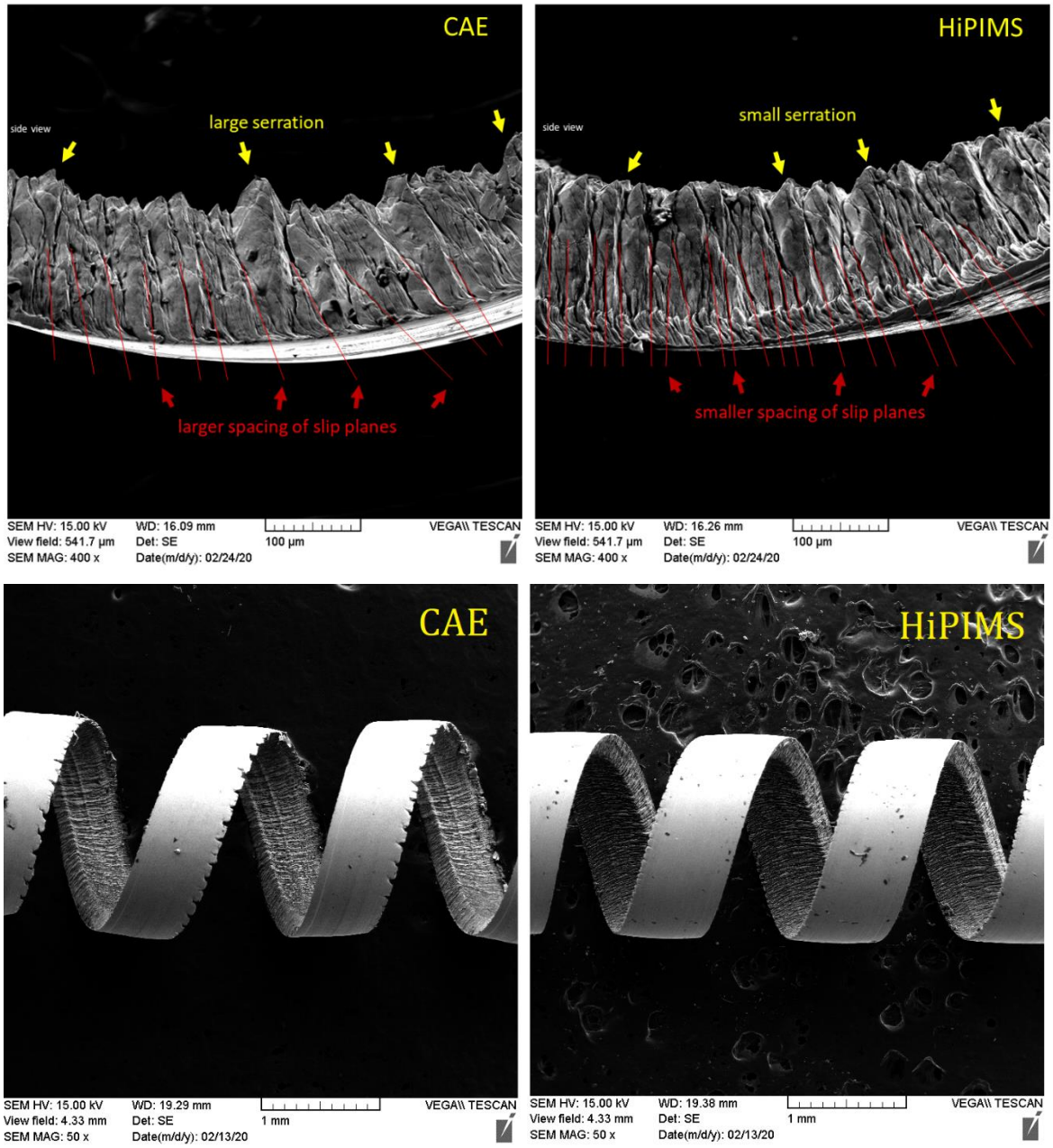

Figure 43 - SEM images of chip of machining Inconel in study A.